

Archives

LB

2322

.A9x

T-841

# Microtubule Nucleation at the Golgi in Breast Cancer Cells

Laura Zahn

# Microtubule Nucleation at the Golgi in Breast Cancer Cells

A Thesis

Presented to

The College of Graduate Studies

Austin Peay State University

In Partial Fulfillment

Of the Requirements for the Degree

Master of Science in Biology

Laura Zahn

May 2, 2016

Copyrighted © 2016

By

Laura Zahn

All Rights Reserved

To the College of Graduate Studies:

We are submitting a thesis written by Laura Zahn entitled "Microtubule Nucleation at the Golgi in Breast Cancer Cells." We have examined the final copy of this thesis for form and content. We recommend that it be accepted in partial fulfillment of the requirements for the degree of Master of Science in Biology.

---

Sarah Lundin-Schiller

Research Committee Advisor/Chair

---

Karen Meisch

Committee Member

---

Gilbert Pitts

Committee Member

Accepted for the Graduate and Research Council

Raja Dakshinamurthy

Dean, College of Graduate Studies

(Original signatures are on file with official student records.)

## Statement of Permission to Use

In presenting this thesis in partial fulfillment of the requirements for the Masters of Science in Biology at Austin Peay State University, I agree that the library shall make it available to borrowers under the rules of the library. Brief quotations from this field study are allowable without special permission, provided that accurate acknowledgement of the source is made. Permissions for extensive quotation or reproduction of this field study may be granted by my major professor, or in his/her absence, by the Head of the Interlibrary Services when, in the opinion of either, the proposed use of the material is for scholarly purposes. Any copying or use of the material in this thesis for financial gain shall not be allowed without my written permission.

---

Laura Zahn

---

Date

# LIST OF FIGURES

## FIGURE

## PAGE

1. Control MCF-7 cells seen in <b>(A)</b> phase contrast (40x) and <b>(B)</b> confocal (60x) with $\alpha$ -tubulin (red) and DNA (blue) labeled .....	20
2. Golgi distribution in MCF-7 cells .....	21
3. Control MDA-MB-231 cells seen in <b>(A)</b> phase contrast (40x) and <b>(B)</b> confocal (60x) with $\alpha$ -tubulin (red) and DNA (blue) labeled .....	22
4. Control MDA-MB-231 cell showing migratory morphology .....	22
5. Failed attempts to disassemble microtubules in MCF-7 cells .....	24
6. MCF-7 cells after successful MT disassembly .....	25
7. Microtubule regrowth in MCF-7 cells following MT disassembly (5h nocodazole + 30m ice + 4m regrowth) .....	26
8. MDA-MB-231 cells after complete MT disassembly .....	27
9. Microtubule regrowth in MDA-MB-231 cells following MT disassembly via 40 min ice incubation + 40 sec regrowth .....	28
10. Microtubule regrowth in MDA-MB-231 cells following MT disassembly via 4h nocodazole incubation + 60s regrowth .....	29
11. Average proportion of $\alpha$ -tubulin (red) colocalization with GM130 (green) in MT regrowth experiments .....	31
12. Average proportion of GM130 (green) colocalization with $\alpha$ -tubulin (red) in MT regrowth experiments .....	31
13. Average proportion of GM130 (green) colocalization with EB1 (blue) in MT regrowth experiments .....	32
14. Average proportion of EB1 (blue) colocalization with GM130 (green) in MT regrowth experiments .....	32
15. Control MCF-7 cell stained for <b>(A)</b> $\alpha$ -tubulin <b>(B)</b> GM130 and <b>(C)</b> $\gamma$ -tubulin .....	33
16. EGF-treated MCF-7 cell stained for <b>(A)</b> $\alpha$ -tubulin <b>(B)</b> GM130 and <b>(C)</b> $\gamma$ -tubulin .....	34

## ABSTRACT

LAURA A. ZAHN. Microtubule Nucleation at the Golgi in Breast Cancer Cells. (Under the direction of DR. SARAH LUNDIN-SCHILLER.)

Microtubules (MTs) are cytoskeletal filaments vital to numerous cell processes, including intracellular transport, cell polarity and motility. Microtubules are dynamic and respond to molecular cues by quickly decreasing or increasing in length. Microtubules must be generated from a nucleating source known as a MT-organizing center (MTOC), of which centrosomes are the most well-characterized. More recently, Efimov *et al.* (2007) described non-centrosomal MT nucleation at the Golgi in a human retinal pigment epithelial cell line. Their work has shown that Golgi-derived MT arrays are essential to directionally persistent cell migration and vesicle transport. The first objective of this study was to compare MT nucleation sites in an invasive breast cancer cell line (MDA-MB-231) to those of a non-invasive breast cancer cell line (MCF-7), with the hypothesis that only the migratory invasive cells exhibit MTs originating from the Golgi. Methods included disassembling MTs and allowing slight regrowth so individual nucleation sites could then be seen via fluorescently tagged antibodies ( $\alpha$ -tubulin, *cis* Golgi marker GM130, and EB1—a MT plus-end binding protein) and confocal microscopy. The second objective of this thesis research was to determine if MT nucleation at the Golgi is more apparent during active migration compared to when cells are stationary. Specifically, this was done by inducing migration using the chemoattractant epidermal growth factor (EGF), and then looking for colocalizations between the Golgi,  $\alpha$ -tubulin, and  $\gamma$ -tubulin—a requirement for MT nucleation. This was done with the hypothesis that actively migrating cells will exhibit more MT nucleation at the Golgi than stationary cells. Images were analyzed qualitatively for color overlap, and quantitatively using Manders Colocalization Coefficients. Differences between

groups were tested for significance using one-way ANOVAs and Tukey's post-hoc test. For the MT nucleation portion of this study, results have shown significantly higher colocalization values (coloc) in the highly invasive MDA-MB-231 cells ( $\alpha$ -tubulin coloc GM130=0.39, GM130 coloc  $\alpha$ -tubulin=0.82, GM130 coloc EB1=0.24, and EB1 coloc GM130=0.38) compared to the weakly invasive MCF-7 cells (0.15, 0.08, 0.02, 0.16, respectively). For the migration study, EGF-treated cells exhibited higher colocalization values than control cells for three of the four protein combinations tested, but EGF-treated MDA-MB-231 cells exhibited significantly higher values ( $\alpha$ -tubulin coloc GM130=0.20, GM130 coloc  $\alpha$ -tubulin=0.89, and  $\gamma$ -tubulin coloc GM130=0.47) than both control groups as well as the treated MCF-7 cells. Overall, these results indicate MT nucleation at the Golgi occurs more frequently in the invasive MDA-MB-231 cell line compared to the weakly invasive MCF-7 cells. The presence or absence of Golgi-derived MTs may help to explain the difference in migratory potential commonly exhibited by these two cell lines.

# TABLE OF CONTENTS

CHAPTER I .....	1
Introduction and Literature Review .....	1
Introduction.....	1
Microtubule Structure and Function .....	2
Microtubule Nucleation .....	4
Golgi Apparatus Structure and Function.....	5
Golgi-derived Microtubules.....	6
Cell Migration and Chemotaxis .....	9
Metastatic Breast Cancer .....	10
Study Objectives .....	11
CHAPTER II.....	13
Cell Types .....	13
MCF-7 Breast Cancer Cells .....	13
MDA-MB-231 Breast Cancer Cells.....	14
CHAPTER III .....	15
Materials and Methods.....	15
Cell culture.....	15
MT Depolymerization and Recovery .....	15
Extraction Buffer and Fixation .....	16
EGF-Induced Migration.....	17
Immunofluorescence .....	17
Microscopy and Image Acquisition .....	18
Colocalization and Statistical Analysis.....	18
CHAPTER IV .....	20
Results.....	20
General Observations.....	20
Microtubule Disassembly and Regrowth in MCF-7 Cells .....	23
Microtubule Disassembly and Regrowth in MDA-MB-231 Cells.....	27
Colocalization for Regrowth Experiments.....	30
EGF-Induced Migration in MCF-7 Cells.....	33

EGF-Induced Migration in MDA-MB-231 Cells ..... 36

Colocalization for Migration Experiments..... 39

CHAPTER V ..... 42

Discussion and Conclusions ..... 42

Golgi Distribution in MCF-7 Cells ..... 42

Microtubule Disassembly ..... 43

MT Nucleation at the Golgi ..... 44

Future Implications ..... 46

Conclusions..... 47

LITERATURE CITED ..... 48

APPENDIX A: Photographs..... 58

APPENDIX B: Data Tables ..... 65

17. Control MDA-MB-231 cell stained for (A) $\alpha$ -tubulin (B) GM130 and (C) $\gamma$ -tubulin .....	37
18. EGF-treated MDA-MB-231 cell stained for (A) $\alpha$ -tubulin (B) GM130 and (C) $\gamma$ -tubulin .....	38
19. Average proportion of $\alpha$ -tubulin (red) colocalization with GM130 (green) for EGF experiments .....	40
20. Average proportion of GM130 (green) colocalization with $\alpha$ -tubulin (red) for EGF experiments .....	40
21. Average proportion of GM130 (green) colocalization with $\gamma$ -tubulin (blue) for EGF experiments .....	41
22. Average proportion of $\gamma$ -tubulin (blue) colocalization with GM130 (green) for EGF experiments .....	41
23. Additional images of MT regrowth in MCF-7 cells following 5h nocodazole + 30m ice + 4m regrowth .....	58
24. Additional images of MT regrowth in MDA-MB-231 cells following 40m ice + 40s regrowth .....	59
25. Additional images of MT regrowth in MDA-MB-231 cells following 4h nocodazole + 60s regrowth .....	60
26. Control MCF-7 cells used to compare to EGF-treated cells .....	61
27. Additional images of EGF-treated MCF-7 cells .....	62
28. Control MDA-MB-231 cells used to compare to EGF-treated cells .....	63
29. Additional images of EGF-treated MDA-MB-231 cells .....	64

## LIST OF TABLES

TABLE	PAGE
1. List of experimental methods used in the attempt to disassembly all MTs in MCF-7 cells .....	23
2. Colocalization summary table for MT regrowth experiments.....	30
3. Colocalization summary table for MCF-7 EGF-induced migration.....	39
4. Colocalization summary table for MDA-MB-231 EGF-induced migration .....	39
5. Raw colocalization data for the MT disassembly/regrowth experiment .....	65
6. Raw colocalization data for control and EGF-treated MCF-7 cells .....	66
7. Raw colocalization data for control and EGF-treated MDA-MB-231 cells.....	67

# CHAPTER I

## Introduction and Literature Review

### Introduction

There are certain cellular components that are considered fundamental. For example, all eukaryotic cells exhibit a cytoskeleton that, among other roles, serves as both the bones and muscles of a cell, offering them stability, structure, and the capacity to move. All eukaryotic cells also contain membrane bound organelles, such as the Golgi apparatus, with highly specialized structures and functions. Though the basics for these essential cellular parts have been studied for decades, new insights and roles for them continue to emerge. These modern revelations not only expand our understanding of healthy cellular processes, but also mechanisms that can go awry in the diseased state.

The focus of this thesis research has been a novel function of the Golgi apparatus to nucleate the cytoskeletal filaments called microtubules. It is not yet known how universal or widespread this functional ability is, and thus looking for its evidence within different cell types is a useful endeavor. Microtubules that arise from the Golgi, rather than their typical origin at the centrosome, have been shown in other studies to be functionally unique and play a critical role in directed cell migration. This role is particularly interesting as it relates to metastatic cancer, which results from an abnormal capacity for tumor cells to migrate away from their site of origin. Various cancer types exhibit different potentials to migrate and invade, though it is not well understood how such variances in migratory ability arise. The goal of this thesis research was to reveal a potential cause for such differences, specifically the presence or absence of Golgi-derived microtubules.

The remainder of this chapter is a review of the background literature to provide the proper context for this thesis research. Sections describing microtubule structure, function, and nucleation, as well as Golgi apparatus structure and function are provided. This is followed by a section covering what is currently known about microtubules that arise from the Golgi specifically. A discussion of the highly coordinated process of cell migration and chemotaxis is also given, as well as the global problem of metastatic breast cancer. The study objectives that follow this background information provide an outline for the specific hypotheses of this thesis research and the experiments that were done to test them. Chapter 2 provides a detailed description of the two different cell types used for this study followed by Chapter 3, which outlines the materials and methods. Chapter 4 includes the results from all experiments, which are discussed in detail in Chapter 5.

### Microtubule Structure and Function

Microtubules (MTs) are cytoskeletal filaments present in virtually all eukaryotic cells. They are made from protein heterodimers of tubulins  $\alpha$  and  $\beta$ , which form protofilaments by polymerizing end to end so that one dimer's  $\alpha$  subunit attaches to the next dimer's  $\beta$  unit (Alberts *et al.*, 2002). A single MT is formed from multiple protofilaments, typically thirteen, arranged laterally to create a relatively rigid hollow tube. This regular, parallel arrangement creates a MT with  $\alpha$  subunits exposed at one end (called the minus end) and  $\beta$  subunits exposed at the other (called the plus end). Microtubules are very dynamic and respond to molecular cues by adding or releasing these subunits, usually from the plus end, which can cause a rapid change in their overall length.

The rate of MT growth/shrinkage is heavily dependent upon temperature and local

amounts of free tubulin subunits in the cytoplasm (Horio & Murata, 2014). However, individual MTs alter their length to achieve a specific purpose, and thus growing and shrinking MTs coexist simultaneously within the cytoplasm. This phenomenon is known as “dynamic instability” and is characterized by alternating periods of growth, shrinkage, and pausing of the protofilament ends. Free tubulin dimers must bind GTP before they can be added to a growing MT end. The GTP is hydrolyzed to GDP briefly after assembly, though this step lags behind, resulting in a GTP cap on newly formed ends. The GTP hydrolysis step is not a requirement for MT assembly, but the loss of the GTP cap results in spontaneous rapid depolymerization (Carlier *et al.*, 1997).

Microtubules are critical to numerous fundamental cell processes. For example, MTs are the major structural component of cilia and flagella, which are essential for oriented motility and sensory functions in a wide range of unicellular eukaryotes (Mitchell, 2007). They play a critical role in determining cell morphology, especially during cell differentiation (Picone *et al.*, 2010). The arrangement and segregation of chromosomes as a cell divides is absolutely dependent upon microtubules which make up the mitotic spindle (Alberts *et al.*, 2002). Microtubules also serve as tracks for intracellular transport as motor proteins, such as kinesins and dyneins, walk their length carrying vesicles and protein complexes to other destinations within the cell (Lippincott-Schwartz *et al.*, 1995). Even organelles, such as those of the endomembrane system, mitochondria, and ribosomes, rely on MTs for their proper positioning within the cell (Bisbal *et al.*, 2009; Friedman *et al.*, 2010). Finally, MTs are inherently responsible for a cell’s ability to polarize, to define a front and back, and then carry out the highly coordinated process of cell migration (Etienne-Manneville, 2013).

## Microtubule Nucleation

Microtubules must be generated from a nucleated source beginning at a MT-organizing center (MTOC), of which centrosomes are the most well-characterized. Centrosomes are composed of a pair of centrioles surrounded by a nebulous pericentriolar matrix containing numerous proteins critical to cell cycle control, centrosome structure, and microtubule nucleation (Alberts *et al.*, 2002). From their centrosome-embedded minus ends, MTs spread out in symmetric arrays as their plus-ends grow in response to cellular signals.

Microtubule nucleation requires  $\gamma$ -tubulin, which is a homologue of  $\alpha$  and  $\beta$  tubulins and is nearly ubiquitous throughout the eukaryotic domain (Kollman *et al.*, 2011). In multicellular eukaryotes,  $\gamma$ -tubulin exists, for the most part, as a component of larger protein conglomerates called  $\gamma$ -tubulin ring complexes ( $\gamma$ -TuRCs) (Oegema *et al.*, 1999). These ring complexes are so named because of their open ring-like structure, which has a diameter very close to that of a microtubule (Zheng *et al.*, 1995). Studies in a wide variety of eukaryotes have established the highly conserved nature of  $\gamma$ -TuRCs and their pivotal role in MT nucleation both *in vivo* and *in vitro* (Moritz *et al.*, 1995; Zheng *et al.*, 1995; Vogel *et al.*, 1997; Murphy, Urbani, and Stearns, 1998). Studies using direct immune-negative stain electron microscopy and 3D electron-microscopic tomography have found  $\gamma$ -TuRCs to associate specifically with the extreme minus ends of MTs, providing strong evidence for the “template” model which proposes that  $\gamma$ -TuRCs function as a template guide at the base of newly formed MTs within MTOCs (Keating and Borisy, 2000; Moritz *et al.*, 2000).

Though the most common, centrosomes are not the only MTOC described to date. The main MTOC in fungi, for example, is a structure called the spindle pole body which remains embedded in the nuclear envelope (Kollman *et al.*, 2011). Vascular plants lack centrosomes but

are capable of nucleating MT from both the nuclear membrane and from  $\gamma$ -tubulin complexes bound to stable MT bundles in the cell cortex (Schmit, 2002; Murata *et al.*, 2005). Microtubules that make up the axoneme of cilia and flagella are nucleated from basal bodies at their base (Kobayashi and Dynlacht, 2011). Pigment granules in fish melanophore fragments lacking centrosomes are capable of nucleating MTs in a dynein dependent manner (Malikov *et al.*, 2004). In *C.elegans* intestinal cells, MTOC function transfers from the centrosome to the apical membrane after the fourth round of cell divisions early in development (Feldman and Priess, 2012). A number of studies have also implicated the Golgi apparatus as a MTOC in some mammalian cell types, which was the inspiration for this thesis work (Chabin-Brion *et al.*, 2001; Efimov *et al.*, 2007; Oddoux *et al.*, 2013).

### Golgi Apparatus Structure and Function

The Golgi apparatus is a highly dynamic organelle present in all eukaryotic cells as part of the secretory pathway. Its structure consists of a stack of flattened disc-shaped membranes, called cisternae, which are connected via proteinaceous bridges (Cluett and Brown, 1992) rather than extensions of the lipid bilayer as previously thought (Bracker *et al.*, 1971; Tanaka *et al.*, 1986). There are usually four to six cisternae within a Golgi stack in mammalian cells, but there can be as many as 60 in some unicellular flagellates (Alberts *et al.*, 2002). In some types of cells, like the secretory tissues of plants, there can be several hundred Golgi stacks per cell (Hua and Graham, 2000-2013). In most animal cells though, the Golgi is found as a single-copy organelle arranged in a compact perinuclear configuration in close proximity to the centrosome.

The Golgi serves as the cell's molecule processing center where highly organized, sequential reactions occur within each of its parts (Hua and Graham, 2000-2013). The *cis* Golgi

faces the endoplasmic reticulum (ER) and serves as the entry area for newly synthesized lipids and proteins carried in vesicles budding from the ER. These molecules are sorted and moved through the different cisternae while undergoing a series of covalent modifications. These changes typically involve the addition, change, or removal of oligosaccharide chains to lipids and proteins, which can serve as final destination markers for these molecules, or function in signaling regulation and cell-to-cell recognition, among other things (Alberts *et al.*, 2002). In their final form, molecules are sorted again and packed within vesicles that bud from the *trans* Golgi which are then carried along MTs to their final destinations. These locations include lysosomes, the cell membrane, or an earlier compartment of the Golgi or ER. These finished molecules can also be highly concentrated within secretory vesicles that are released from the cell in regulated bursts.

Given the importance of MTs in the transport of vesicles entering and exiting the Golgi, it should come as no surprise that MT minus ends are routinely found in close proximity to the Golgi (Rogalski and Singer, 1984). Indeed, the entire structure of the Golgi seems dependent upon intact MTs. Studies employing the MT depolymerizing drug nocodazole routinely cause the Golgi apparatus to scatter into mini-stacks distributed throughout the cytoplasm (Cole *et al.*, 1996; Alberts *et al.*, 2002). Moreover, the clustering of these fragmented pieces after the drug is washed away is facilitated by MTs alone, independent of any other cytoskeletal filament (Ho *et al.*, 1989).

### Golgi-derived Microtubules

The first evidence of direct MT nucleation at the Golgi came in 2001 by Chabin-Brion *et al.* in a study using nocodazole to completely depolymerize MTs in cultured hepatocytes. MTs

were allowed to briefly recover, revealing colocalizations between Golgi fragments and newly growing MTs in fixed stained cells. This study also found purified Golgi membranes could support MT nucleation given purified tubulin and GTP. Furthermore, their purified Golgi membranes were shown to contain significant amounts of  $\gamma$ -tubulin, a critical protein in MT nucleation.

More recently, MT nucleation at the Golgi has also been documented to occur in a human retinal pigment epithelial (RPE-1) cell line, even after laser ablation of the centrosome. Evidence of this was provided by Efimov *et al.* (2007) who developed a method to trace MTs back to their point of origin via time-lapse imaging and fluorescently labeled end-binding protein 3 (EB3) which attaches to the growing ends of MTs. Interestingly, this study also shows that Golgi-derived MT arrays are intrinsically asymmetric with a preference towards the leading cell edge in motile cells. Generation of these Golgi-derived arrays is dependent upon the presence of two accessory proteins: cytoplasmic linker associated proteins (CLASPs) which coat the entire length of these non-centrosomal MTs during their initial growth phase, and a trans-Golgi network specific coiled-coil protein called GCC185. This study also showed that removal of GCC185 via siRNA caused CLASPs to no longer localize to the Golgi, though CLASPs could facilitate MT formation even when not bound to the Golgi membranes. Nevertheless, CLASPs must associate with the Golgi to ensure non-centrosomal MTs are properly anchored and stabilized for normal use within the cell.

The obvious question this new discovery raises is: Do these Golgi-derived MTs exhibit functional abilities unique from their centrosomal counterparts? Microtubules are known to play a critical role in intracellular transport and in facilitating proper positioning of membrane-bound organelles. A study by Miller *et al.* (2009) looked at the role of Golgi-derived MTs in

establishing Golgi organization, which after cell division begins as Golgi mini-stacks that later associate to form a continuous ribbon of interconnected stacks of flat cisternae. This study shows that Golgi mini-stacks are able to form without the influence of MTs but their proper assembly into a Golgi ribbon is dependent upon the presence of Golgi-derived MTs. They were also able to demonstrate that cells depleted of their CLASP-dependent MTs or overexpressing GFP-CLASP2C displayed randomized vesicle trafficking rather than the polarized trafficking seen in controls. In addition, their research also showed that in CLASP-depleted cells as well as cells overexpressing GFP-CLASP2C migration was random as opposed to the directionally oriented movement seen in control cells. This indicated that CLASP-dependent Golgi-derived MTs are essential to directionally persistent vesicle transport and migration.

Hurtado *et al.* (2011) employed a truncated version of the centrosome/Golgi apparatus associated protein AKAP450 transfected into RPE-1 cells and found that this caused the AKAP450 to dissociate from the Golgi apparatus. This was also found to specifically inhibit Golgi-derived MT nucleation while centrosomal nucleation was unaffected. A subsequent experiment was performed to analyze Golgi apparatus reassembly following nocodazole washout in control cells and those expressing two truncated versions of AKAP450, AK1B and AK1. Results indicated that the AK1B fragment produced a broken but properly positioned Golgi ribbon, while the AK1 fragment caused a correctly formed Golgi ribbon to be randomly malpositioned. This malpositioning of the Golgi was then shown to disrupt directed cell migration, leading to the conclusion that proper Golgi positioning is required for the polarization needed to direct cell migration.

## Cell Migration and Chemotaxis

Cell migration is a requirement for multiple processes including development, immune responses, and tissue regeneration (Alberts *et al.*, 2002). Abnormal cell migration can cause a number of pathological conditions including cancer cell metastasis and invasion. Chemotaxis is the migration of cells in response to a chemical stimulus, and typically occurs in a directed orientation. For cells to migrate, polarization of the cell must first occur to establish a front and back, or a leading and trailing edge. This is accomplished through gradients of molecular signals such as Rho family GTPases, namely Cdc42, Rac1, and RhoA, which in turn trigger dramatic changes to the actin cytoskeleton. Microtubules are critical to this process because they help establish the distribution of these signal gradients. For example, RhoA is regulated by the nucleotide exchange factor GEF-H1, which is specifically activated by MT depolymerization and rendered inactive when bound to MTs (Krendel *et al.*, 2002). Microtubules also transport vesicles and needed molecules directly. For example, the Arp 2/3 complex is an actin-polymerization nucleator in leading cell protrusions of migrating cells, and is composed of seven protein subunits. To ensure this complex is in the right place at the right time, the seven mRNAs needed are brought to the leading cell protrusions by microtubules where they are then translated and assembled in direct proximity to where they function (Mingle *et al.*, 2005). This kind of mRNA localization is thought to ensure a high concentration of the subunits locally which promotes their assembly into the larger protein complex. It also bypasses the diffusion constraints that would otherwise be associated with random assembly in the cytoplasm followed by targeted transport to their site of action.

Microtubules also regulate cell migration by controlling the dynamics of focal adhesions (FAs), which are leverage sites the cell uses to push or pull itself across the substrate (Etienne-

Manneville, 2013). For example, MTs deliver integrins and other FA assembly proteins to nascent FAs in the leading cell edge (Bretscher and Velasco, 1998). Simultaneously, other MTs target mature FAs in the rear, literally poking at them repeatedly, which correlates with FA disassembly (Kaverina *et al.*, 1999). Though the precise mechanism of how MTs cause FA disassembly is not yet understood, it is thought to occur by locally modifying Rho GTPase signaling pathways (Stehbens and Whitman, 2012). Nonetheless, FA disassembly is required for the trailing edge to retract, allowing the migrating cell to move forward.

### Metastatic Breast Cancer

Metastasis is the spread of cancer cells from their origin site in one organ or tissue to another that is not directly connected with it. This process requires a sequence of complex steps, beginning with the detachment of cancer cells from the primary tumor, and their migratory invasion through the basement membrane into the surrounding tissue (Hunter *et al.*, 2008). From there, they must find a way to enter the microvasculature of the blood or lymph system, and manage to survive the hemodynamic shear forces in the circulation away from their home microenvironment (Dong *et al.*, 2005). They must then successfully exit the vasculature, invade a new host tissue, and proliferate in this foreign environment (Stoletov *et al.*, 2010). Their ability to do all of this while avoiding apoptosis or triggering an immune response is quite remarkable and still not well understood.

Breast cancer is the most prevalent type of malignancy in women worldwide, with 1.7 million new cases diagnosed in 2012 (IARC & WHO, 2012). When tumors remain localized to the breast tissue, the 5-year relative survival rate is quite high at 98.8% (Howlader, 2015). However, after metastatic spread the survival rate drops to only 26.6%. Interestingly, metastatic

spread in breast cancer follows a distinct pattern in that metastases are more common in certain organs, like lymph nodes, bone marrow, liver, and lung, but less frequent in others, including kidneys, skin, and pancreas (Mukherjee and Zhao, 2013). Studies have shown that certain growth factors and small peptide molecules called chemokines are released from these common organ sites and can act as chemoattractants for breast cancer cells. For example, the chemokine receptor C-X-C chemokine receptor type 4 (CXCR4) is upregulated in some types of breast cancers, and its ligand CXCL12, also known as stromal derived factor 1- $\alpha$  (SDF-1 $\alpha$ ), is most highly expressed in the organs of first metastatic spread (Muller *et al.*, 2001). Binding of CXCL12 to its receptor induces actin polymerization and pseudopodia formation, leading to chemotactic migration. Similarly, epidermal growth factor (EGF) is expressed in a variety of health tissues, including brain, bone marrow, and lung, and has also been shown to be a strong chemoattractant for breast cancer cells. When EGF binds to its cell surface receptor (EGFR), a tyrosine kinase is activated which starts a number of signaling pathways involved in proliferation and migration (Voldborg, 1997). A study by Kim *et al.* (2013) also found SDF-1 $\alpha$  and EGF to work cooperatively to induce directed cell migration. However, why some breast cancer types are more likely to respond to these signals than others, despite equivalent receptor expression, remains to be revealed.

### Study Objectives

The first objective of this thesis research was to look for evidence of MT nucleation at the Golgi in two human breast cancer cell types with different migratory potentials. Specifically, this was done by depolymerizing MTs and allowing brief regrowth to reveal any colocalizations between the Golgi,  $\alpha$ -tubulin, and EB1—a MT plus-end binding protein. This work utilized

MCF-7 cells, which are considered weakly-invasive with a low migratory potential, and MDA-MB-231 cells, which are significantly more motile and invasive. Given that Golgi-derived MTs are critical for directed cell migration, this work was done to test the hypothesis that the invasive MDA-MB-231 cells exhibit MTs originating from the Golgi while the MCF-7 cells do not.

The second objective of this thesis research was to determine if MT nucleation at the Golgi is more apparent during active migration compared to when cells are stationary.

Specifically, this was done by inducing migration using the chemoattractant epidermal growth factor (EGF), and then looking for colocalizations between the Golgi,  $\alpha$ -tubulin, and  $\gamma$ -tubulin—a requirement for MT nucleation. This was done to test the hypothesis that actively migrating cells exhibit more MT nucleation at the Golgi than stationary cells.

## CHAPTER II

### Cell Types

#### MCF-7 Breast Cancer Cells

MCF-7 cells, named after the Michigan Cancer Foundation and the seventh attempt of Herbert Soule to generate a stable cancer cell line, were originally isolated from a metastatic pleural effusion site derived from a mammary gland tumor (Soule *et al.*, 1973). These cells have been described in nearly 25,000 published studies, rivaled in popularity only by the HeLa cell line (Lee, Oesterreich, and Davidson, 2015). They have been particularly useful in breast cancer research because they consistently maintain high expression levels of estrogen receptor alpha (ER $\alpha$ ), a feature found in over half of all human breast cancers (Ali and Coombes, 2000). Their study has led to increased understanding of proliferation in response to estrogen and the development of ER-targeted therapies for breast cancer treatment. In culture, MCF-7 cells are nonmotile and regularly form dense clumps with numerous desmosomes tightly connecting cells to one another (De Bruyne *et al.*, 1988; Holliday and Speirs, 2011). *In vitro* migration studies consistently report low invasion rates for MCF-7 cells (Bozzuto *et al.*, 2015; Nieman *et al.*, 1999), though some studies have shown chemoattractants, such as epidermal growth factor (EGF, 10 ng/ml), can induce invasion in these cells in a chemotaxis chamber experiment (Sun *et al.*, 2005). However, 50 ng/ml EGF did not stimulate MCF-7 invasion in an under-agarose cell migration assay (Khajah *et al.*, 2006). This feature of generally low migratory potential made these cells particularly useful for this thesis research.

## MDA-MB-231 Breast Cancer Cells

The MDA-MB-231 cell line was one of 19 human breast carcinoma cell lines derived from patients at M.D. Anderson Hospital and Tumor Institute, and like MCF-7 cells, originated from a metastatic pleural effusion site (Cailleau, Olivé, and Cruciger, 1978). In their original characterization, MDA-MB-231 cells were described as spindle-shaped cells that lack estrogen receptors and spread randomly, rather than forming dense epithelial sheets. They also lack progesterone receptors and human epidermal growth factor receptor 2 (HER-2) (Subik *et al.*, 2010), making them “triple-negative” like approximately 10-15% of all breast cancers, and thus insensitive to the receptor targeted treatments currently available for other breast cancer types (Chavez *et al.*, 2012; Chen and Russo, 2009). Triple negative breast cancer is particularly aggressive, and the MDA-MB-231 cell line is no exception. Not only are they fast growing, but also highly invasive, as demonstrated in numerous *in vitro* assays (scratch/wound healing, 2-D and 3-D Boyden/transwell chambers, microchemotaxis chamber, biomimetic electrospun nanofiber 3D environments) (Bozzuto *et al.*, 2015; Nieman *et al.*, 1999; Price *et al.*, 1999; Nelson *et al.*, 2014) as well as *in vivo* (Patsialou *et al.*, 2009). It was this high migratory potential that made the MDA-MB-231 cell line of particular interest for this thesis research.

## CHAPTER III

### Materials and Methods

#### Cell culture

Both cell types were acquired from American Type Culture Collection (ATCC; MDA-MB-231, catalog #HTB-26 and MCF-7, catalog #HTB-22) and were grown in complete media containing Dulbecco's Modified Eagle's Medium (DMEM) (ATCC, catalog #30-2002) supplemented with 10% fetal bovine serum (ThermoFisher Scientific, catalog #10082-139), and 2% antibiotic/antimycotic (ThermoFisher Scientific, catalog #15240-096). Cells were grown in 75-mm<sup>2</sup> seed flasks until confluent, usually within 5 to 7 days for MDA-MB-231 cells, and 7 to 10 days for MCF-7 cells. Cells were then removed from the seed flask via 5 minute incubation with 0.5% trypsin-EDTA in phosphate buffered saline (PBS, pH 7.0). At the end of 5 minutes, fresh medium was added to stop the trypsin reaction, and the resulting medium-trypsin-cell solution was centrifuged for approximately 7-8 minutes. The resulting pellet was resuspended using 5 ml of fresh complete media, which was then used to start a new seed flask or divided into 35-mm glass bottom dishes (MatTek, catalog #P35G-1.0-14-C) at approximately 100,000 cells per dish for experiments. Some dishes were treated with poly-L-lysine (Sigma-Aldrich, catalog #P4707) to help keep cells adhered throughout experiments. Cells were maintained at 37°C in 5% CO<sub>2</sub> in air.

#### MT Depolymerization and Recovery

To better visualize the MT nucleation sites, the existing MT array had to first be depolymerized and then allowed to regrow briefly. This allowed detection of nucleation events that would otherwise be obstructed from sight by the entire MT network. To depolymerize the

MTs, the ice recovery assay outlined by Grimaldi *et al.* (2014) was used as a starting point. This procedure involved incubating the 35-mm glass bottom dishes containing live cells on ice for 40 minutes, based on the premise that cold treatment can depolymerize MTs. This proved effective for the MDA-MB-231 cells, but not for the MCF-7 cells. The nocodazole washout procedure described by Zhu and Kaverina (2011) was then attempted, which employed 2 hours incubation in 8  $\mu$ M nocodazole (Sigma-Aldrich, catalog #M1404)—an anticancer drug known to interfere with the polymerization of MTs. This method also left many MTs intact in MCF-7 cells, and increased incubation times in 10  $\mu$ M nocodazole were also tested (3 hours-26 hours) with poor results. Ultimately, the only method that proved successful for completely depolymerizing MTs in MCF-7 cells was 5 hours of 10  $\mu$ M nocodazole treatment, followed by five rinses in media, and 30 minutes of ice incubation. Conversely, 4 hours of 10  $\mu$ M nocodazole treatment alone was sufficient for depolymerizing MTs in MDA-MB-231 cells.

For cells whose MTs were allowed to recover after disassembly, medium was removed and replaced with warm medium (37°C), and the dish placed on a plastic tray floating on a water bath set to 41°C (thermocouple measured top of tray to be 37°C) for the specified time (20-300 seconds).

### Extraction Buffer and Fixation

To improve MT clarity, an extraction buffer was used to reduce the amount of free tubulin within cells while allowing bound tubulin to remain. As suggested by Ochoa *et al.* (2011), the extraction buffer was made using 80 mM PIPES (Sigma-Aldrich, catalog #P1851), pH 6.8, 1 mM EGTA (Sigma-Aldrich, catalog #E3889), 1 mM  $MgCl_2$  (J.T. Baker, catalog #1-2444) (PEM buffer), supplemented with 0.5% Triton-X (Fisher Scientific, catalog #BP151-100) and 25%

(wt/vol) glycerol (Sigma-Aldrich, catalog #G5516) immediately before use. Extraction buffer was kept on ice for at least 30 minutes before use. Immediately after the regrowth time, media were removed from the cells and replaced with 1 ml of ice cold extraction buffer. Cells were left on the bench top in the cold extraction buffer for 5 minutes, rinsed once with extraction buffer, and then immediately subjected to fixation in ice cold anhydrous methanol (99.8%, Sigma-Aldrich, catalog #322415). Fixation occurred at  $-20^{\circ}\text{C}$  for five minutes, followed by three five minute rinses in PBS. Cells were left in PBS at least overnight to rehydrate before staining.

### EGF-Induced Migration

To induce migration, cells were first placed in serum-free media overnight. The following morning, 20 ng/ml EGF (PeproTech, catalog #AF-100-15) was added to the media. Cells were periodically checked over the next eight hours for morphological changes indicative of migration. After eight hours, cells were fixed using cold anhydrous methanol at  $-20^{\circ}\text{C}$  for five minutes, and rinsed in PBS three times for five minutes each.

### Immunofluorescence

To each plate of fixed cells, 1-2 ml of blocking buffer containing PBS, 5% horse serum (ThermoFisher Scientific, catalog #16050-130) and 1% bovine serum albumin (BSA; Sigma-Aldrich, catalog #A7034), was added and incubated for 40 minutes to one hour at room temperature. Primary antibodies included monoclonal rat anti- $\alpha$ -tubulin (YL1/2, ThermoFisher Scientific, catalog #MA1-80017; 1:800), polyclonal rabbit anti-GM130 (cis-Golgi matrix protein, ThermoFisher Scientific, catalog #PA1-077; 1:800), monoclonal mouse anti-EB1 for the disassembly/regrowth experiments (MT plus end-binding protein; 1A11/4, ThermoFisher

Scientific, catalog #41-2100; 1:5000), and monoclonal mouse anti- $\gamma$ -tubulin for the migration experiments only (ThermoFisher Scientific, catalog #MA1-850; 1:50). Cells were incubated with primary antibodies sequentially for one hour each at room temperature and then washed three times for five minutes each, using fresh PBS each time. Secondary antibodies included anti-rat Alexa-Fluor 568, anti-rabbit Alexa-Fluor 488, and anti-mouse Alexa-Fluor 405 (ThermoFisher Scientific catalog #s A-11077, A-21206, A-31553; 1:500 each). Secondary antibodies were incubated with cells simultaneously for one hour at room temperature covered with foil to protect from light. The cells were then washed three times for five minutes, using fresh PBS each time. In some experiments, the nucleus was labeled using a few drops of Hoechst 33258 (ThermoFisher Scientific, catalog #H1398; 1 mg/15 ml) added to cells for five minutes at room temperature, followed by three five minute rinses in PBS.

### Microscopy and Image Acquisition

After staining, cells were imaged using a Nikon Eclipse Ti inverted laser scanning confocal microscope equipped with Plan Apo 60x 1.4 numerical aperture oil immersion objective. Z-stacks with 0.125  $\mu$ m steps were acquired using NIS Elements Advanced Research version 14.3. For MT regrowth experiments, z-stacks from five fields of view containing 10-15 cells each were analyzed. For EGF-induced migration experiments, z-stacks from ten fields of view containing 1-4 cells each were analyzed.

### Colocalization and Statistical Analysis

Z-stacks were evaluated qualitatively for overlap between the different color signals in merged channel images. Colocalization was also analyzed quantitatively using ImageJ (Fiji;

Rasband, 1997-2015) software. First, each z-stack was automatically thresholded using the Moments-preserving bilevel method (Tsai, 1985). Manders Colocalization Coefficients (MCCs) were then calculated for each thresholded z-stack using the JACoP plugin (Bolte and Cordelieres, 2006). The MCC value is calculated as follows: Let A be a color (red, for example) and let B be some other color (green, for example). The MCC value is the proportion of A colocalized with B relative to the total amount of A present ( $MCC = \frac{\Sigma A \text{ coloc } B}{\Sigma A}$ ). This software analyzes each slice in the z-stack individually but then gives a single MCC value for the entire z-stack. For each z-stack, this was done four times, once for each of the color combinations: red colocalizing with green, green colocalizing with red, green colocalizing with blue, and blue colocalizing with green. In the results section, these comparisons are indicated using the respective proteins of interest:  $\frac{\alpha\text{-tubulin coloc GM130}}{\alpha\text{-tubulin}}$ , for example. JMP Pro 10 was then used to calculate all descriptive and inferential statistics for the MCCs. Levene's test was used to test for equal variances between groups. If variances were equal, a one-way ANOVA was used to compare group means. If variances were unequal, a Welch's ANOVA was used. Tukey's post hoc test was used to determine which groups were significantly different from one another.

## CHAPTER IV

### Results

#### General Observations

In our cultures, MCF-7 cells regularly formed rounded, densely compacted clumps of cells (Figure 1). It was often difficult to make out distinct borders between individual cells. After cell division, daughter cells remained adjacent to one another, rarely moving from their point of origin. Staining for the *cis*-Golgi marker GM130 revealed a scattered distribution of Golgi fragments in control MCF-7 cells (Figure 2). This was an unexpected find, as most animal cells tend to have a more compact, perinuclear arrangement of the Golgi. This feature of irregular distribution is not something commonly reported in the literature for MCF-7 cells, but was regularly seen in our experiments.

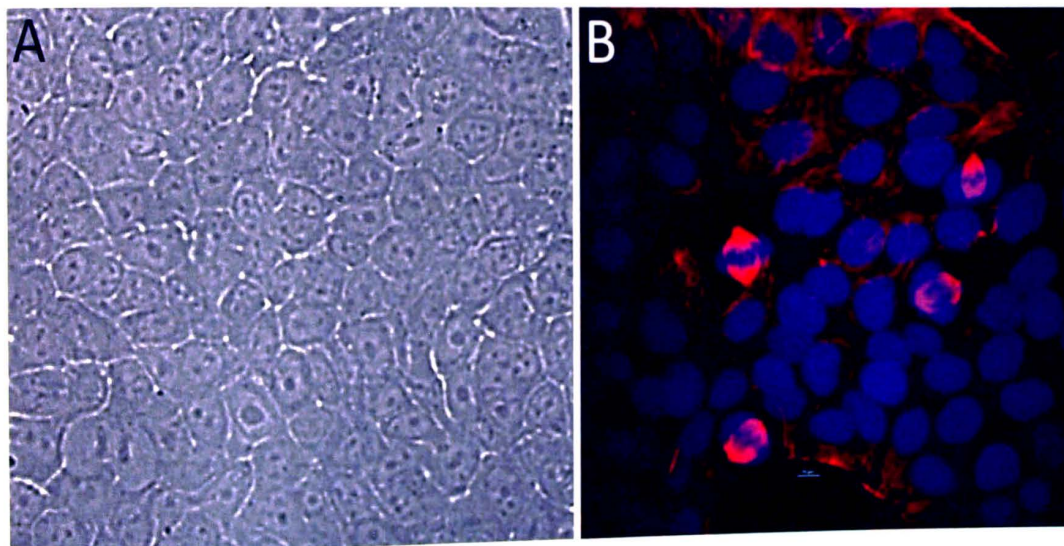


Figure 1. Control MCF-7 cells seen in (A) phase contrast (40x) and (B) confocal (60x) with  $\alpha$ -tubulin (red) and DNA (blue) labeled. These cells form compact clumps, rarely moving away from their origin site. Scale bar represents 10 $\mu$ m.

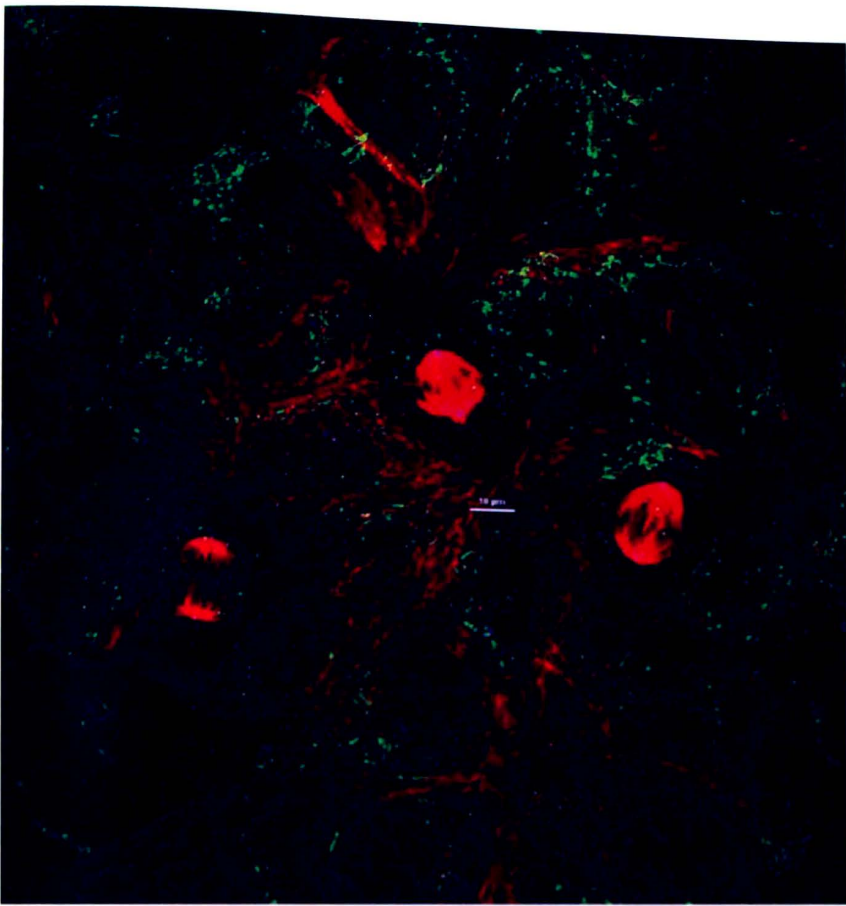


Figure 2. Golgi distribution in MCF-7 cells. Control MCF-7 cells stained for  $\alpha$ -tubulin (red) and GM130 (green). The Golgi appears relatively scattered in both mitotic cells and interphase cells seen here. Scale bar represents 10 $\mu$ m.

In our cultures, MDA-MB-231 cells exhibited a spindle shaped morphology, with cytoplasmic extensions common (Figure 3). These cells grew very rapidly, but existed in a more individualized manner rather than the dense clumps seen in MCF-7 cells. When MDA-MB-231 cells divided, the daughter cells stretched far apart in opposite directions, and rarely stayed in close proximity to one another. Even when unstimulated, cells could often be seen with a distinct leading edge indicative of migratory behavior (Figure 4). When stained for GM130, the Golgi appeared more typical in that it was relatively compact and in close proximity to the nucleus.

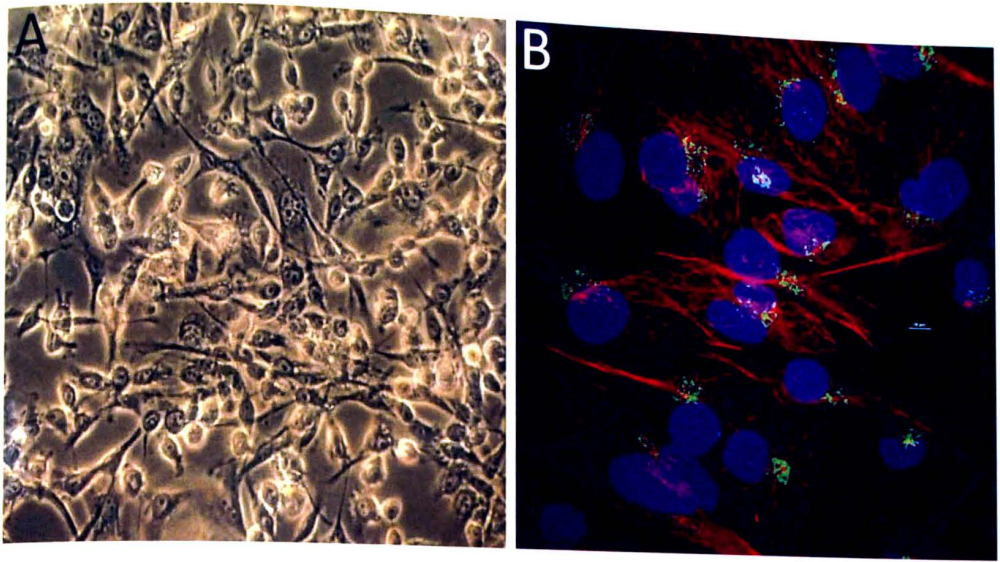


Figure 3. Control MDA-MB-231 cells seen in (A) phase contrast (40x) and (B) confocal (60x) with  $\alpha$ -tubulin (red) and DNA (blue) labeled. These cells are more fibroblast-like, exhibiting numerous cytoplasmic extensions and a more individualized appearance. Scale bar represents 10 $\mu$ m.

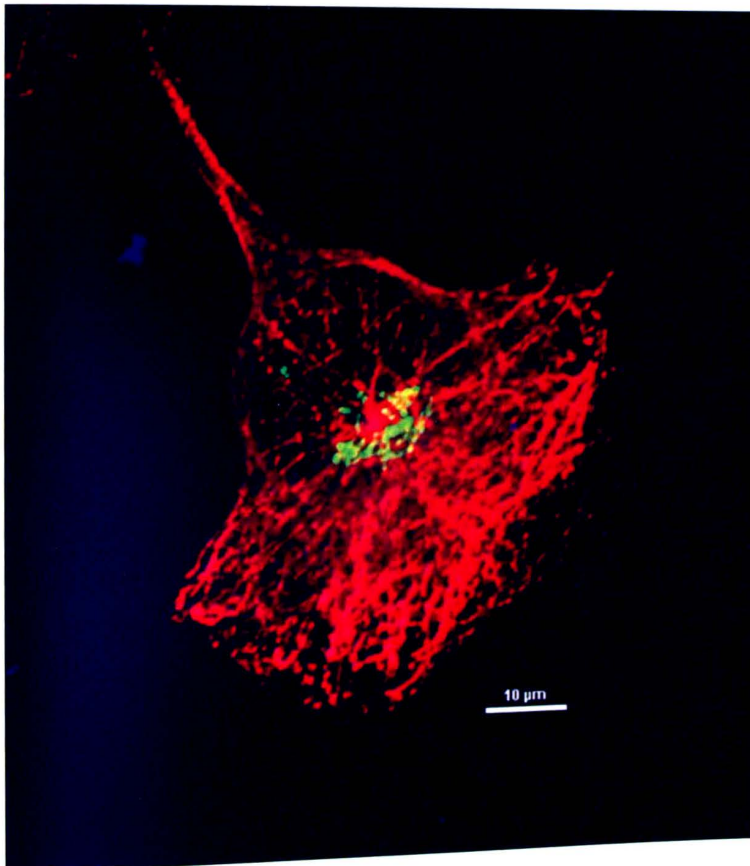


Figure 4. Control MDA-MB-231 cell showing migratory morphology. Microtubules ( $\alpha$ -tubulin) can be seen in red and the Golgi (GM130) in green. Scale bar represents 10 $\mu$ m.

## Microtubule Disassembly and Regrowth in MCF-7 Cells

Microtubules in MCF-7 cells proved very difficult to experimentally disassemble. Table 1 summarizes the various methods used that proved unsuccessful. Some example images of failed experiments can be seen in Figure 5. The only method that consistently eliminated all MTs in these cells was 5 hour treatment with 10 $\mu$ M nocodazole followed by 5 rinses in fresh media, and 30 minutes on ice (Figure 6). To eliminate free tubulin after disassembly, 5 minutes in ice cold extraction buffer followed by 1 rinse in fresh extraction buffer was necessary.

<b>Experimental Method</b>
40 min ice
45 min ice
2 hour 8 $\mu$ M nocodazole
3 hour 8 $\mu$ M nocodazole
2 hour 10 $\mu$ M nocodazole
4 hour 10 $\mu$ M nocodazole
5 hour 10 $\mu$ M nocodazole
8 hour 10 $\mu$ M nocodazole
12 hour 10 $\mu$ M nocodazole
16 hour 10 $\mu$ M nocodazole
26 hour 10 $\mu$ M nocodazole
5 hour 10 $\mu$ M nocodazole + 30 min ice

Table 1. List of experimental methods used in the attempt to disassembly all MTs in MCF-7 cells. All methods proved unsuccessful except for the last: 5 hour 10 $\mu$ M nocodazole + 30 min ice.

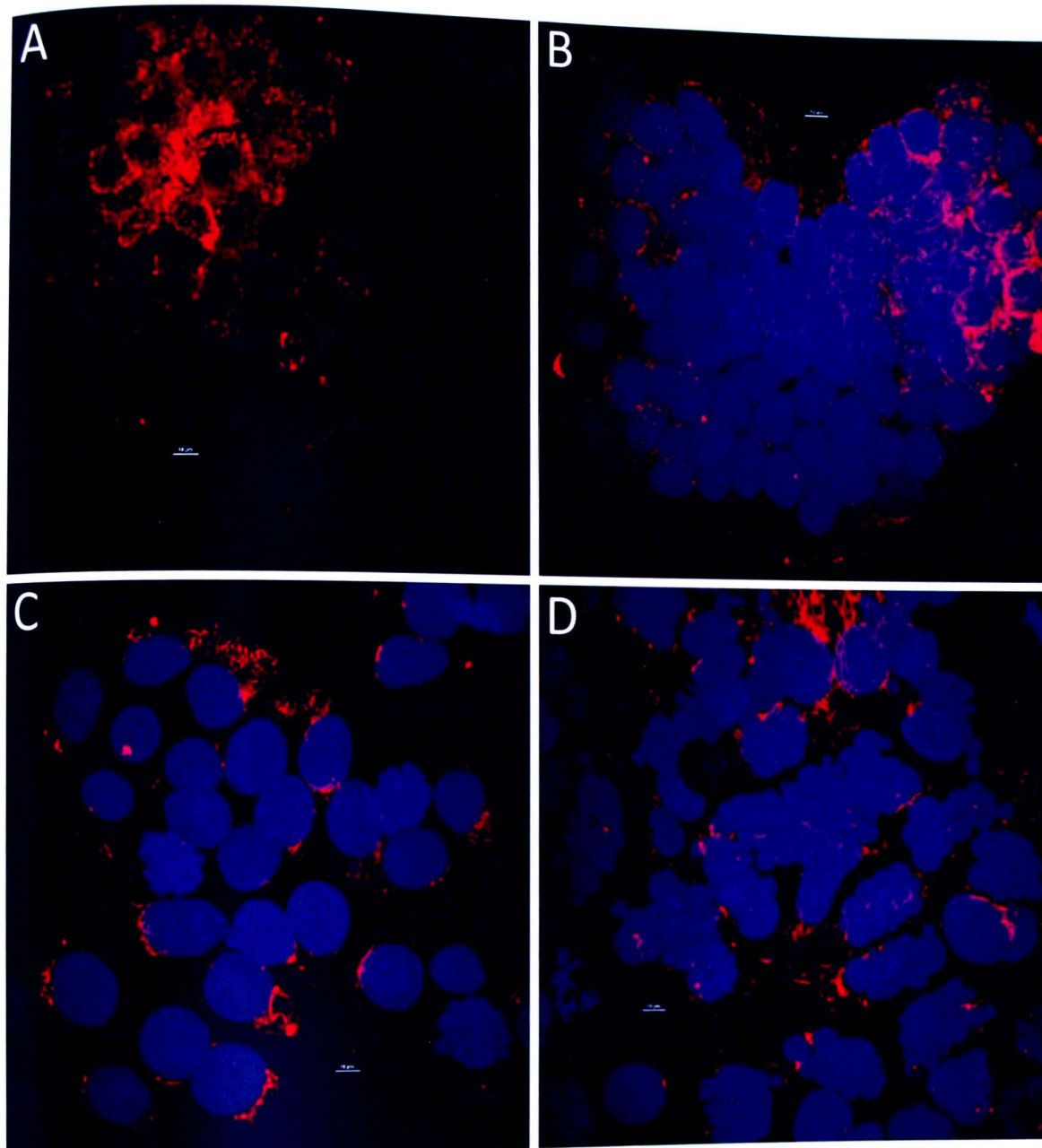


Figure 5. Failed attempts to disassemble microtubules in MCF-7 cells. Max intensity images from z-stacks showing MCF-7 cells after (A) 40m ice incubation (B) 2h 10μM nocodazole incubation (C) 5h 10μM nocodazole incubation and (D) 26h 10μM nocodazole incubation. In all photos DNA is seen in blue and α-tubulin in red. Prolonged incubation in nocodazole can cause mitotic arrest in prophase, as can be seen in some cells in C and D. Scale bars represents 10μm.

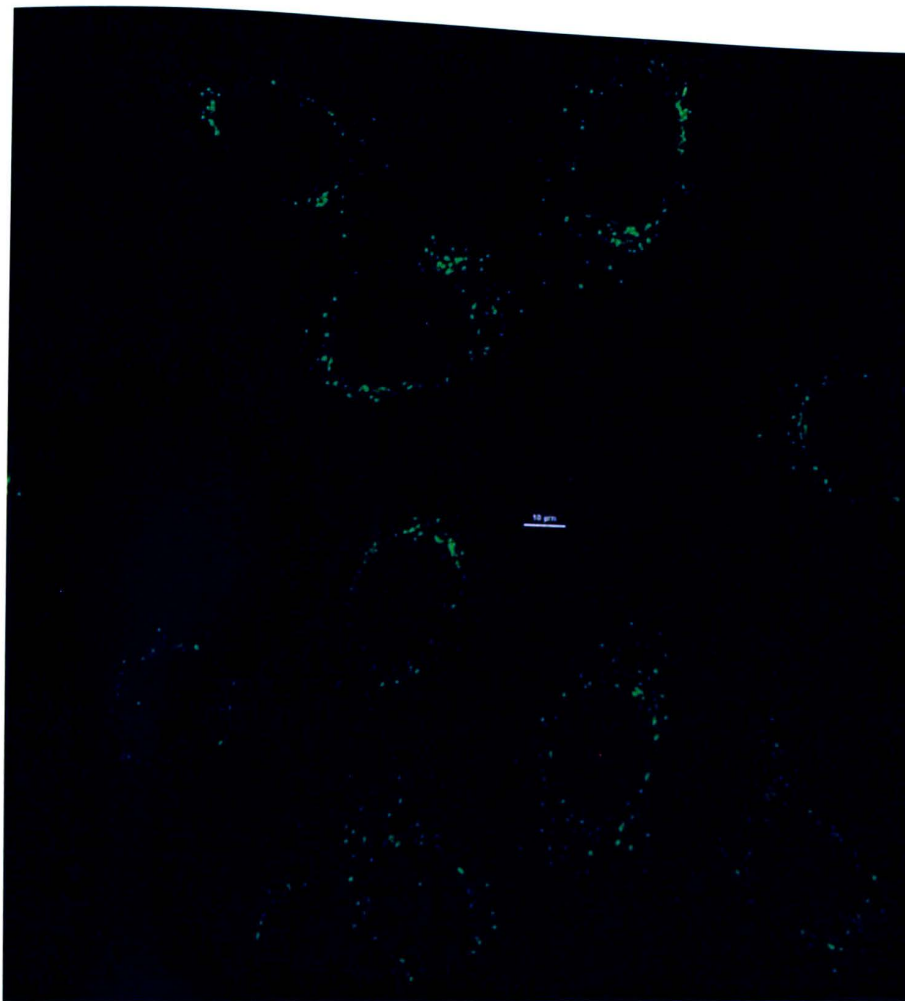


Figure 6. MCF-7 cells after successful MT disassembly. Microtubules were removed in these cells via 5h 10 $\mu$ M nocodazole incubation followed by 5 rinses, 30m ice incubation, 5m extraction buffer incubation, and 1 rinse in fresh extraction buffer. Note the scattered Golgi (green) and the lack of tubulin (red). This is a max intensity projection of a z-stack. Scale bar represents 10 $\mu$ M.

In general, MT regrowth seemed to occur at slightly different rates between experiments, making it difficult to reproduce exactly comparable lengths between cell types. The images used for analysis for MCF-7 cells were after 4 minutes of regrowth (Figure 7), which was a bit longer than it took MDA-MB-231 cells to reach comparable lengths.

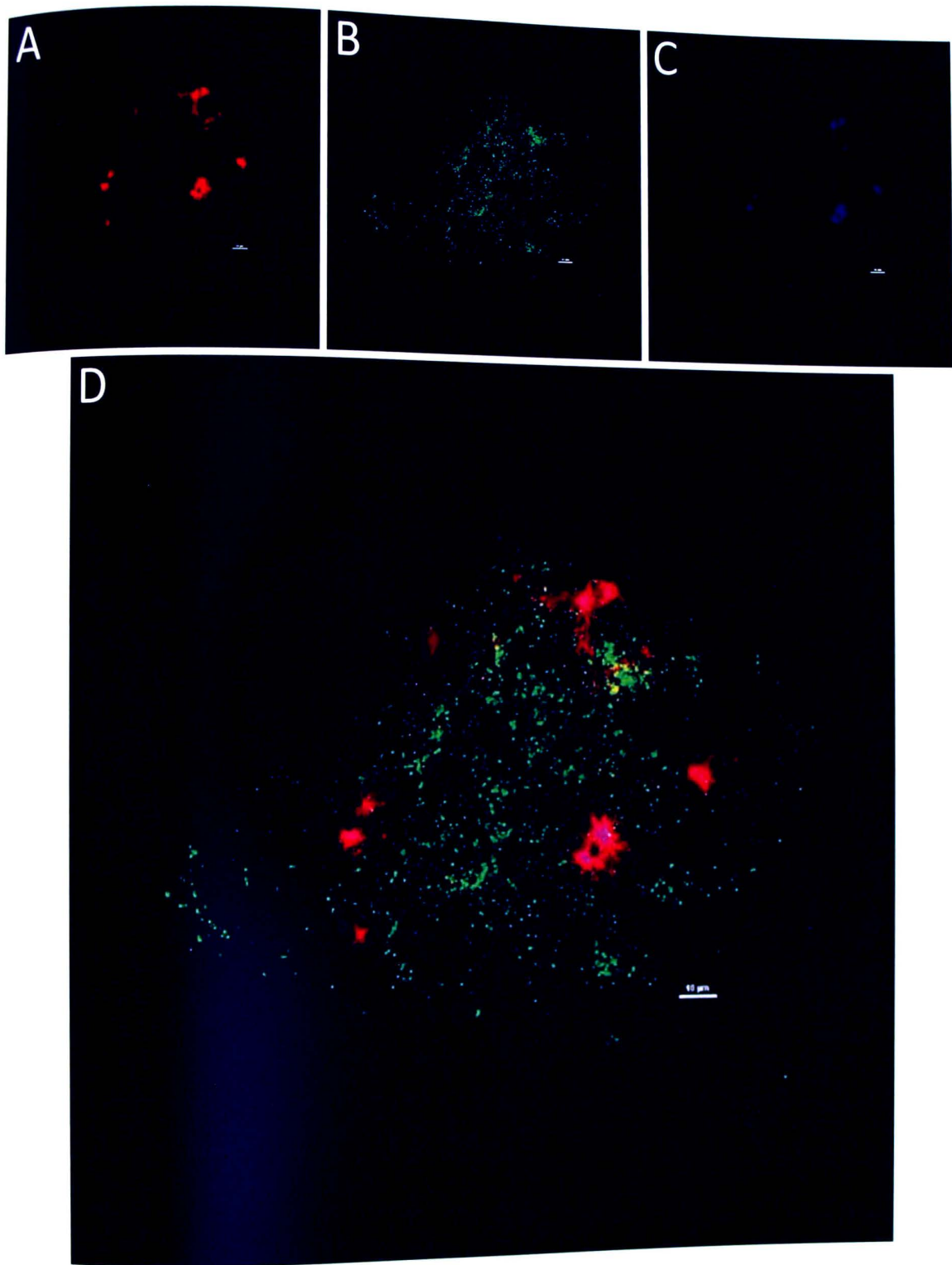


Figure 7. Microtubule regrowth in MCF-7 cells following MT disassembly (5h nocodazole + 30m ice + 4m regrowth). Max intensity images for individual channels can be seen for (A)  $\alpha$ -tubulin (B) GM130 and (C) EB1. (D) Merge of A-C, showing little overlap between the red  $\alpha$ -tubulin and the green Golgi, or between Golgi and blue EB1. Scale bar represents 10  $\mu\text{m}$ .

## Microtubule Disassembly and Regrowth in MDA-MB-231 Cells

MTs in MDA-MB-231 cells proved much easier to disassemble than MCF-7 cells. Forty minutes of ice incubation followed by five minutes in ice cold extraction buffer and one rinse in fresh extraction buffer was sufficient to remove all intact and free tubulin. This method left the Golgi relatively intact, as can be seen in Figure 8. Microtubules were also disassembled using four hour 10  $\mu$ M nocodazole incubation, followed by five minutes in ice cold extraction buffer and one rinse in fresh extraction buffer. This method scattered the Golgi (Figure 8) similar to that seen in MCF-7 cells, and thus both methods were used for analysis.

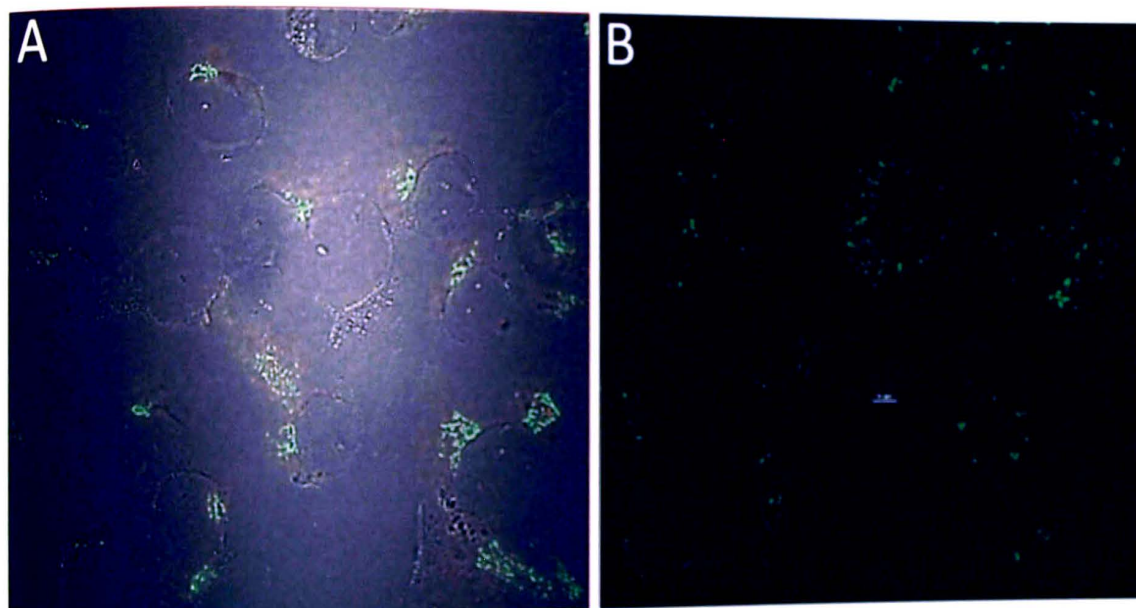


Figure 8. MDA-MB-231 cells after complete MT disassembly. Microtubules were eliminated in these cells via (A) 40m ice incubation or (B) 4h 10 $\mu$ M nocodazole incubation. Note the relatively intact Golgi (green) in A compared to the more dispersed Golgi seen in B. Both treatments successfully eliminated  $\alpha$ -tubulin (red). Both images are max intensity projections. Scale bar represents 10 $\mu$ m.

The images used for analysis for MDA-MB-231 cells were 40 seconds of regrowth following ice treatment, and 60 seconds of regrowth following nocodazole treatment.

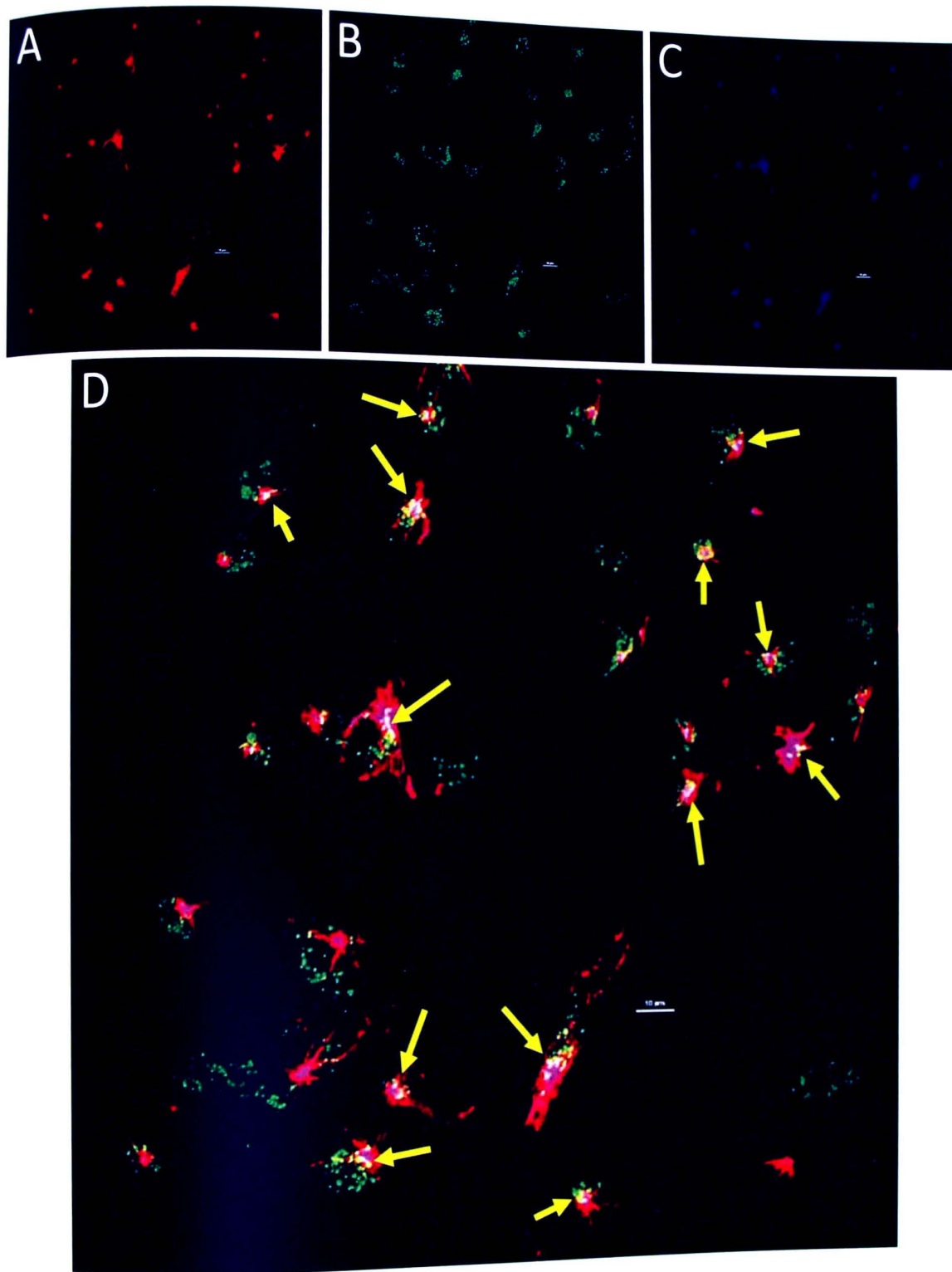


Figure 9. Microtubule regrowth in MDA-MB-231 cells following MT disassembly via 40 min ice + 40 sec regrowth. Max intensity images of individual channels can be seen for (A)  $\alpha$ -tubulin (B) GM130 and (C) EB1. (D) Merge of A-C, showing some overlap between the individual channels, as indicated with yellow arrows. Though this is a max intensity image, overlap was still present within individual slices of the z-stack. Scale bar represents 10  $\mu$ m.

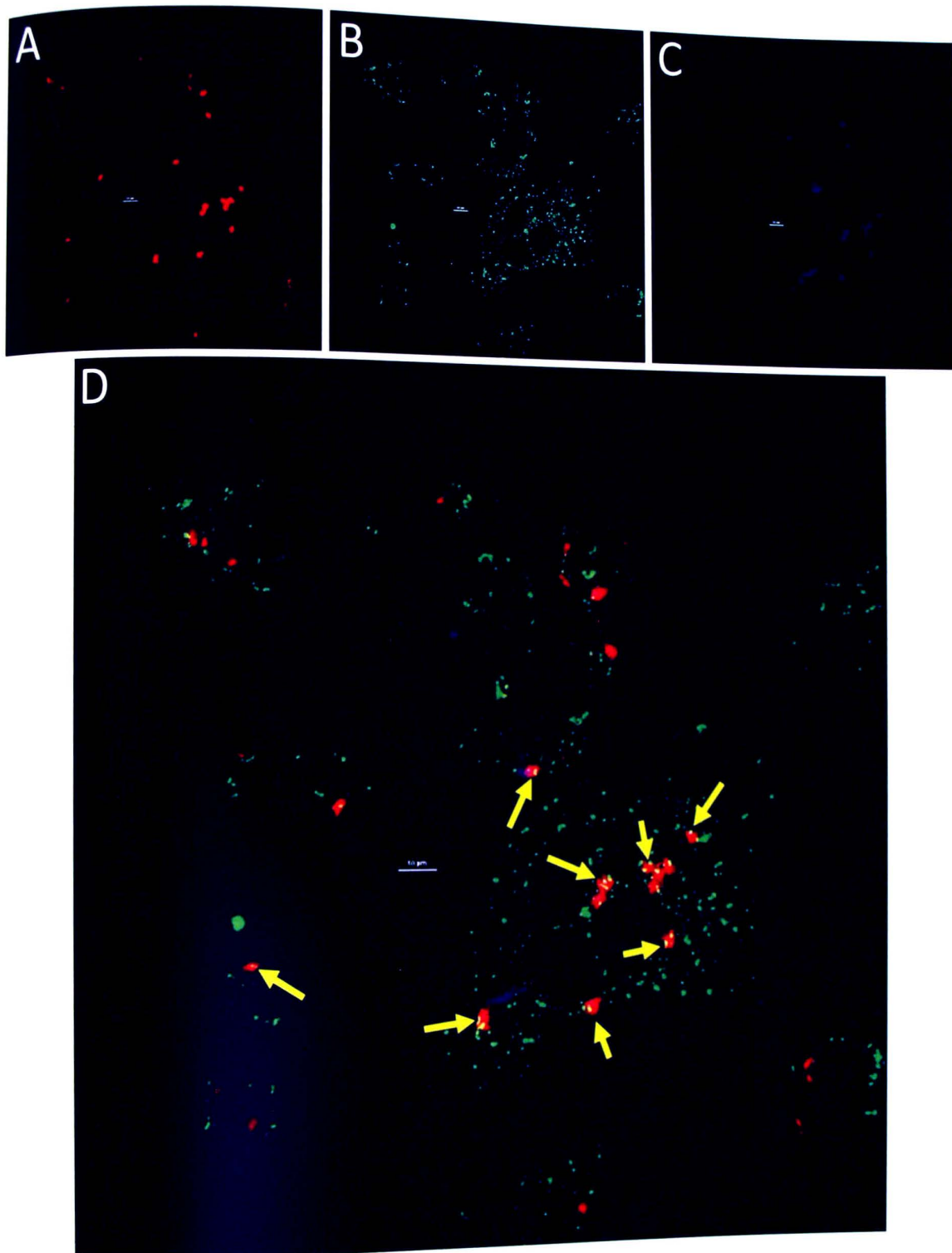


Figure 10. Microtubule regrowth in MDA-MB-231 cells following MT disassembly via 4h nocodazole + 60s regrowth. Max intensity images for individual channels can be seen for (A)  $\alpha$ -tubulin (B) GM130 and (C) EB1. (D) Merge of A-C showing points of overlap between channels, as indicated by arrows. Though this is a max intensity image, overlap was still present within individual slices of the z-stack. Scale bar represents 10  $\mu\text{m}$ .

# Colocalization for Regrowth Experiments

Z-stacks from five fields of view were analyzed for colocalization for each cell group. Although the images shown above and in the appendix are max-intensity images, the JACoP software analysis evaluates color overlap within each individual slice and determines a colocalization value for the entire z-stack. Four colocalization values are produced for each z-stack: red colocalizing with green relative to the total amount of red present; green colocalizing with red relative to the total amount of green present; green colocalizing with blue relative to the total amount of green present; and blue colocalizing with green relative to the total amount of blue present. The group mean and standard deviation for each of these combinations can be seen below in Table 2. All groups had equal variances according to Levene's test, so a one-way ANOVA was used for each comparison (Table 2).















Mander's CC Mean ± STD	α-tubulin coloc GM130 α-tubulin	GM130 coloc α-tubulin GM130	GM130 coloc EB1 GM130	EB1 coloc GM130 EB1
MCF-7 Noco + Ice + 4m regrowth (n=5)	0.15 ± 0.08 	0.08 ± 0.06 	0.02 ± 0.004 	0.16 ± 0.09 
MDA-MB-231 Ice + 40s regrowth (n=5)	0.13 ± 0.08 	0.82 ± 0.11 F=69.6320 P<0.0001* 	0.24 ± 0.15 F=5.3395 P<0.0219* 	0.18 ± 0.09  
MDA-MB-231 Noco + 60s regrowth (n=5)	0.39 ± 0.09 F=16.0516 P<0.0004* 	0.24 ± 0.07 	0.15 ± 0.11  	0.38 ± 0.17 F=5.0604 P<0.0255* 

Table 2. Colocalization summary table for MT regrowth experiments. Average Mander's Colocalization Coefficients and standard deviation results for each color protein combination are shown. Groups were compared using one-way ANOVAs and Tukey's post-hoc test. Within each column, groups with different shapes are significantly different from one another, while those with the same shape are not. Significant p-values are in red.

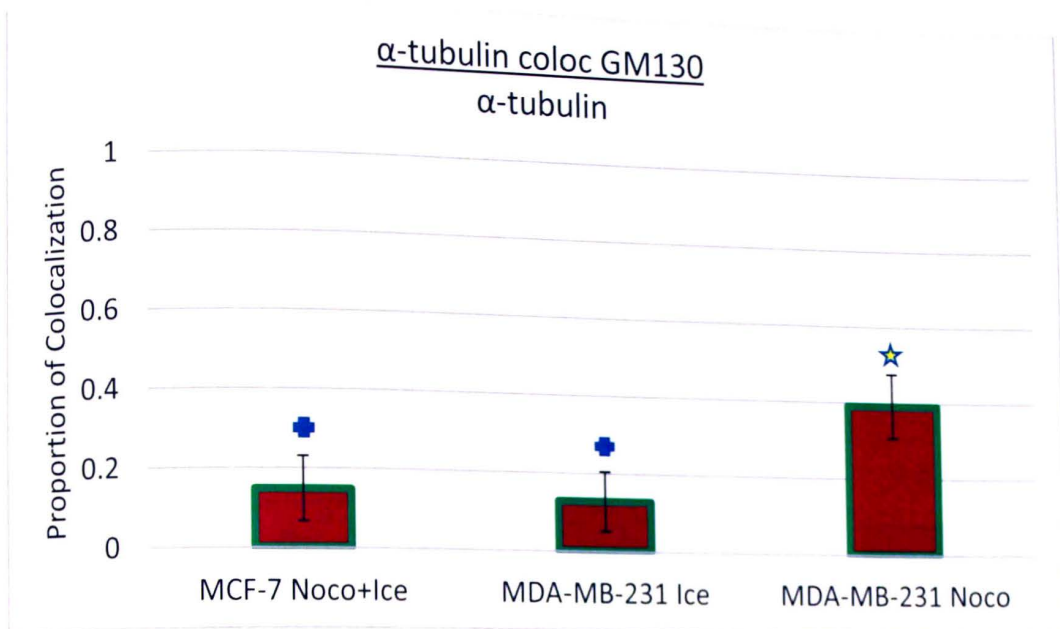


Figure 11. Average proportion of  $\alpha$ -tubulin (red) colocalization with GM130 (green). Error bars reflect standard deviation. Groups with different shapes are significantly different from one another, while groups with the same shape are not. In this case, the nocodazole-treated MDA-MB-231 cells had a significantly higher colocalization value ( $p < 0.0004$ ) than the other two groups.

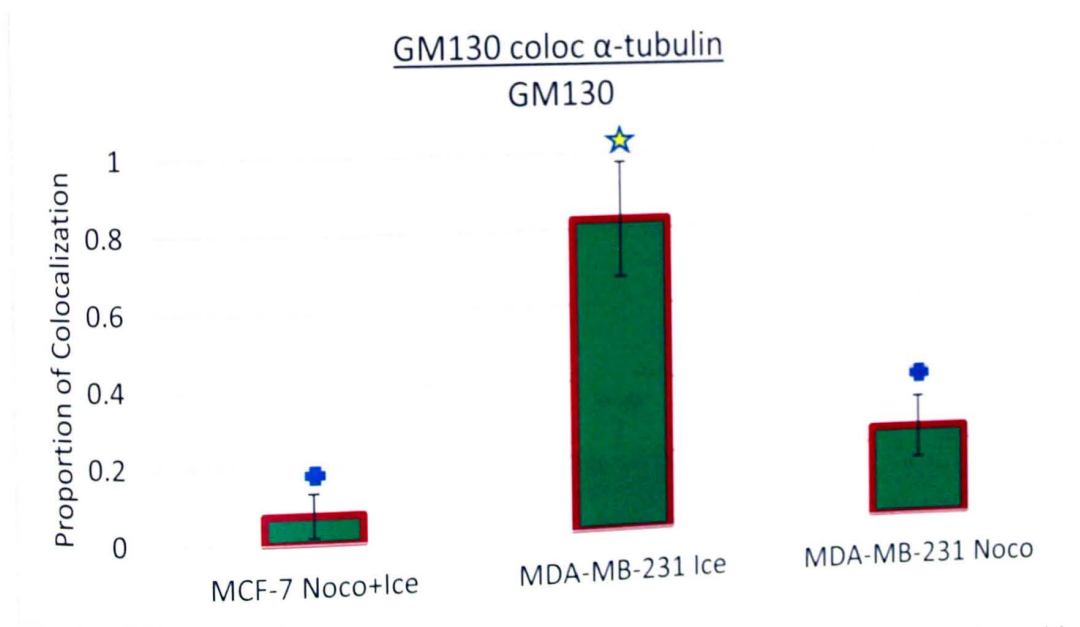


Figure 12. Bar graph showing the average proportion of GM130 (green) colocalization with  $\alpha$ -tubulin (red) for each cell group. Error bars reflect standard deviation. Groups with different shapes are significantly different from one another, while groups with the same shape are not. In this case, the ice-treated MDA-MB-231 cells had a significantly higher colocalization value ( $p < 0.0001$ ) than the other two groups.

### GM130 coloc EB1 GM130

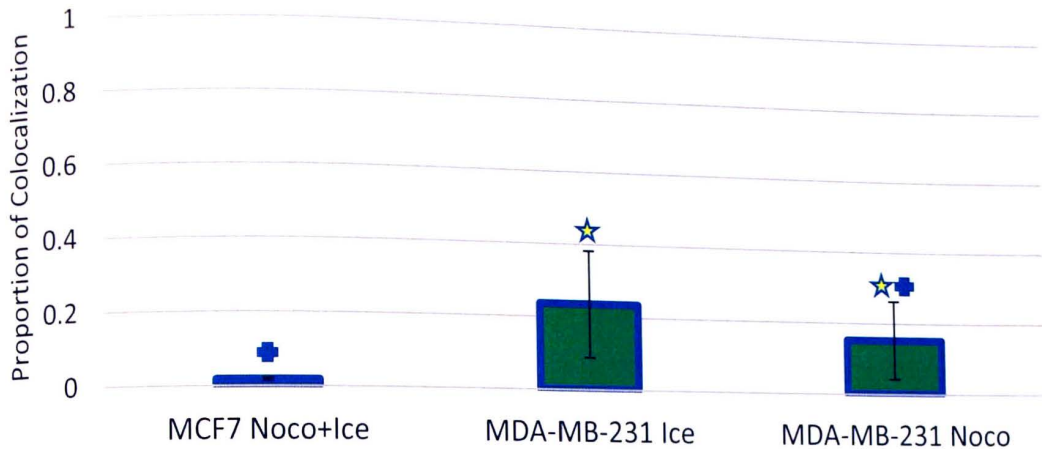


Figure 13. Average proportion of GM130 (green) colocalization with EB1 (blue) for each cell group. Error bars reflect standard deviation. Groups with different shapes are significantly different from one another, while groups with the same shape are not. In this case, the ice-treated MDA-MB-231 cells had a significantly higher colocalization value ( $p < 0.0219$ ) than the MCF-7 cells but not from the nocodazole-treated MDA-MB-231 cells.

### EB1 coloc GM130 GM130

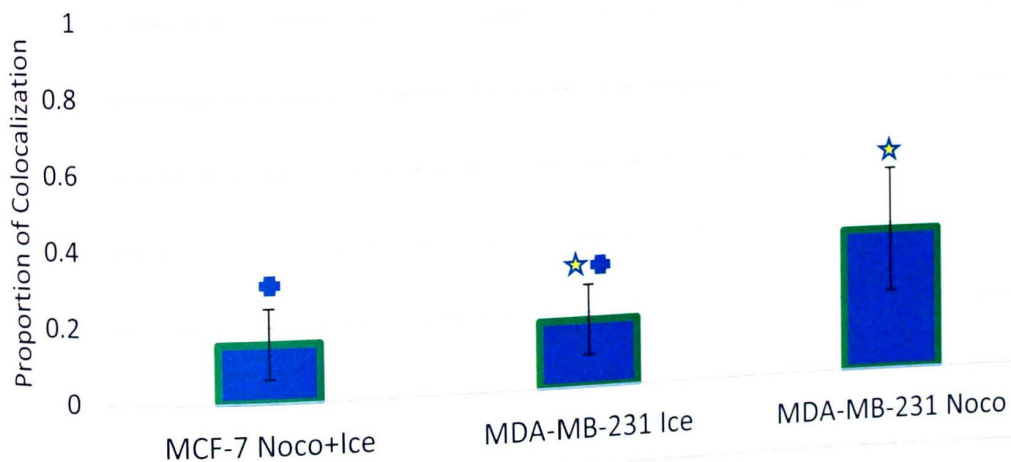


Figure 14. Average proportion of EB1 (blue) colocalization with GM130 (green) for each cell group. Error bars reflect standard deviation. Groups with different shapes are significantly different from one another, while groups with the same shape are not. In this case, the nocodazole-treated MDA-MB-231 cells had a significantly higher colocalization value ( $p < 0.0255$ ) than the MCF-7 cells but not from the ice-treated MDA-MB-231 cells.

## EGF-Induced Migration in MCF-7 Cells

Exposure to EGF induced a prominent morphological change in many of the MCF-7 cells. In contrast to the densely packed sheets of rounded cells seen in control plates, EGF-treated cells began detaching from one another as they spread out across the dish. Many individual cells took on a stellate morphology, exhibiting cytoplasmic extensions in numerous directions. The Golgi distribution in the EGF-treated MCF-7 cells still appeared generally scattered. Though many cells had obviously moved from their site prior to EGF exposure, they still never seemed to properly polarize and display a definitive leading edge. Little overlap could be seen between their green Golgi and blue  $\gamma$ -tubulin (Figure 16).

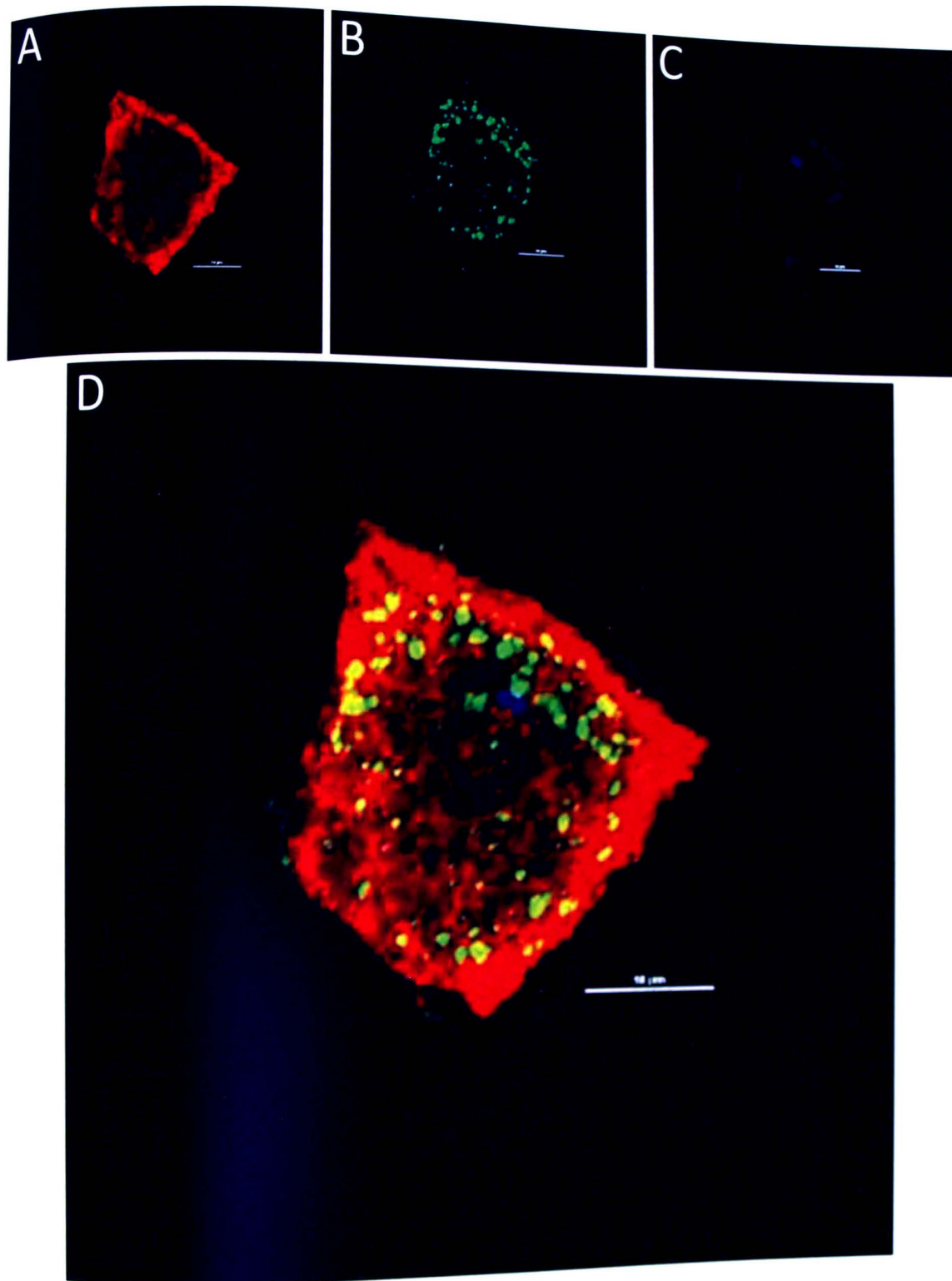


Figure 15. Control MCF-7 cell stained for (A)  $\alpha$ -tubulin (B) GM130 and (C)  $\gamma$ -tubulin. (D) Merge of A-C shows little overlap between the blue  $\gamma$ -tubulin and the green scattered Golgi. Again, these are max intensity images from a z-stack. Scale bar represents 10  $\mu\text{m}$ .

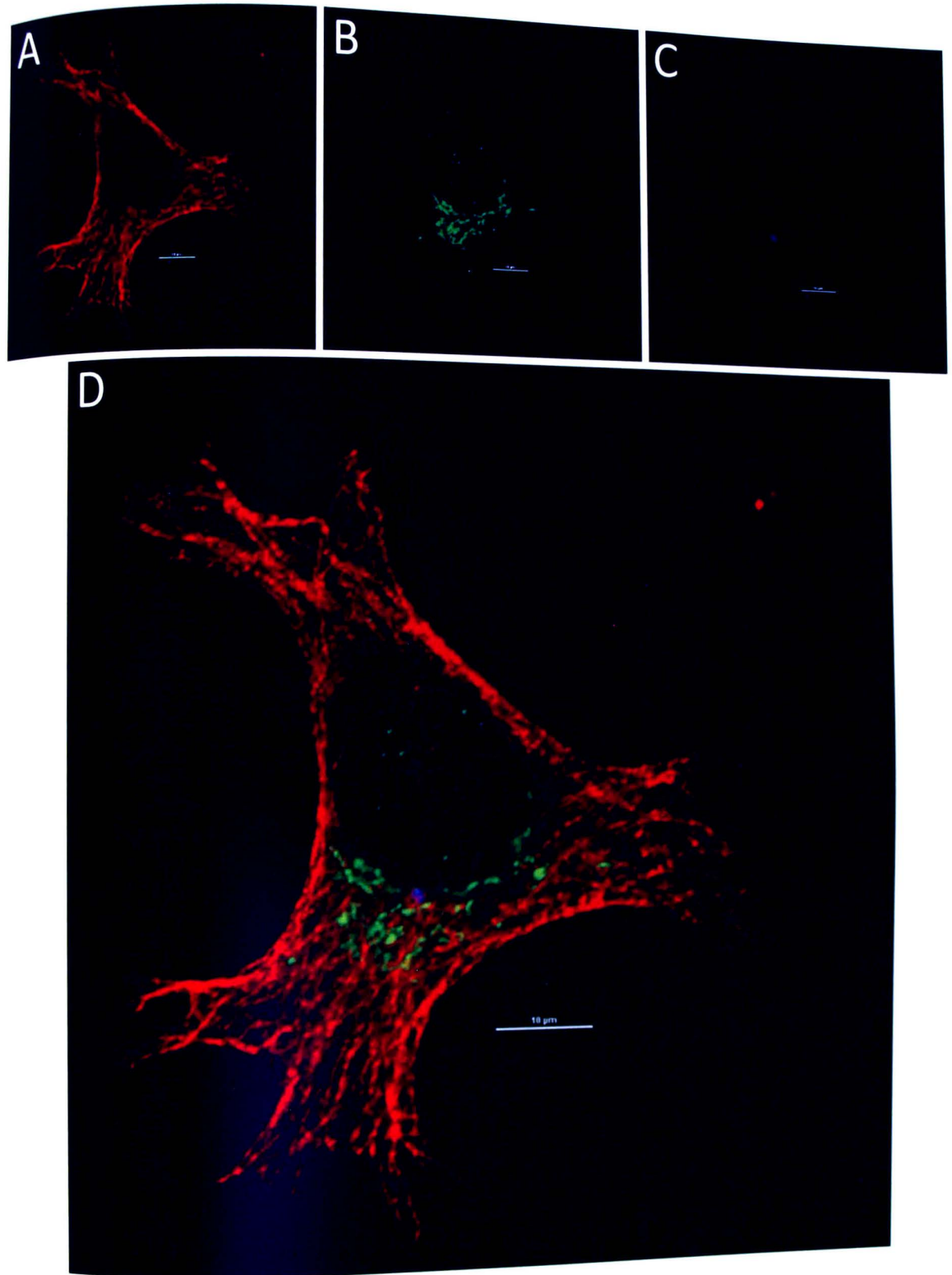


Figure 16. EGF-treated MCF-7 cell stained for (A)  $\alpha$ -tubulin (B) GM130 and (C)  $\gamma$ -tubulin. (D) Merge of A-C shows little overlap between the blue  $\gamma$ -tubulin and the green scattered Golgi. Again, these are max intensity images from a z-stack. Scale bar represents 10  $\mu\text{m}$ .

## EGF-Induced Migration in MDA-MB-231 Cells

Control MDA-MB-231 cells commonly exhibited a migratory morphology in culture, and thus exposure to EGF did not have as dramatic of an effect on cell shape as it did for the MCF-7 cells. Nonetheless, treated MDA-MB-231 cells did appear to migrate more, given that they were more widely dispersed in the dish after EGF exposure. Most treated cells displayed a polarized morphology with the Golgi on one side of the nucleus, usually oriented towards its leading cell edge. In some cells, considerable overlap could be seen between the green Golgi and the blue  $\gamma$ -tubulin (Figure 18).

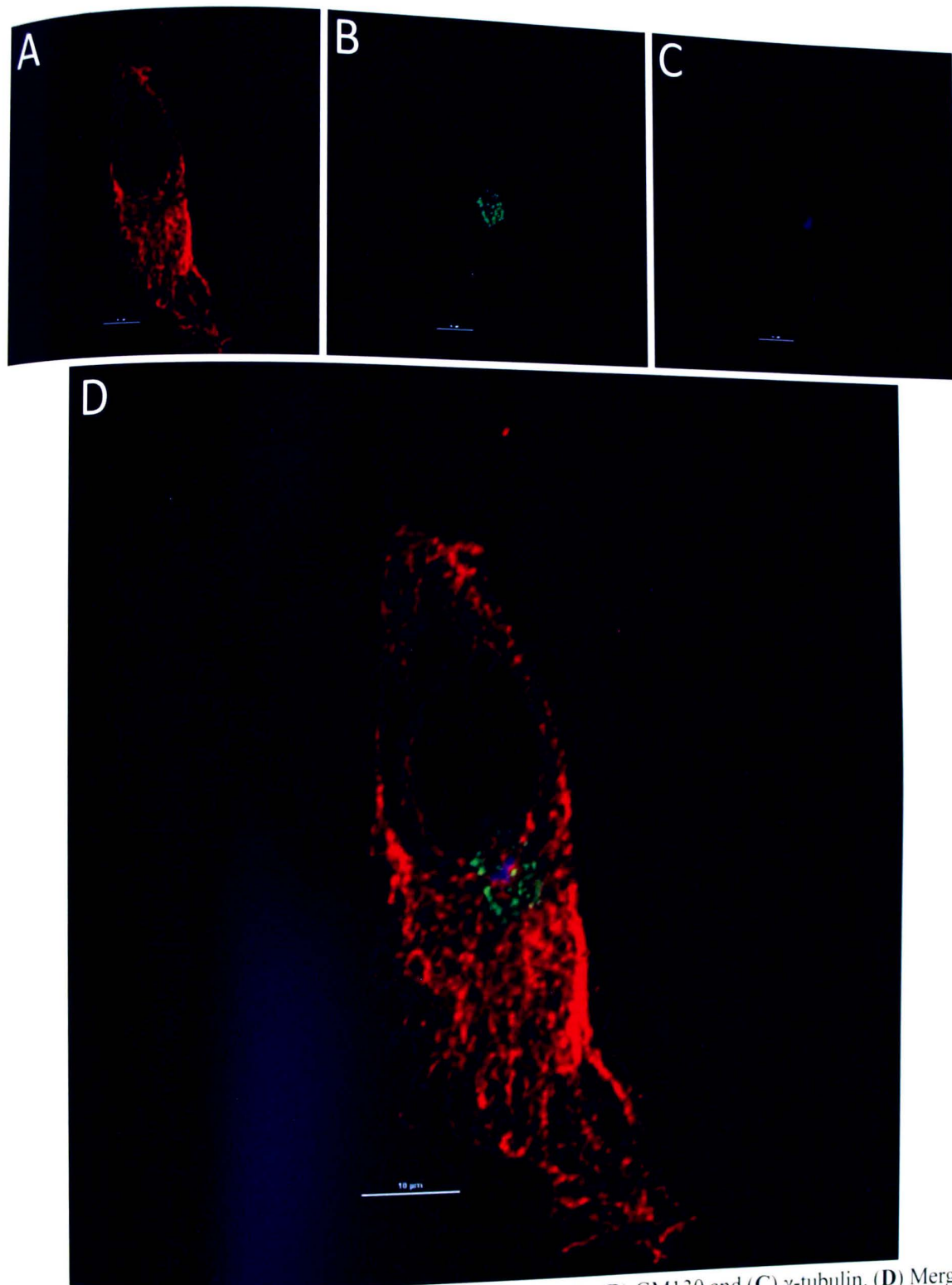


Figure 17. Control MDA-MB-231 cell stained for (A)  $\alpha$ -tubulin (B) GM130 and (C)  $\gamma$ -tubulin. (D) Merge of A-C shows minor overlap between the blue  $\gamma$ -tubulin and the green Golgi. Scale bar represents 10  $\mu\text{m}$ .

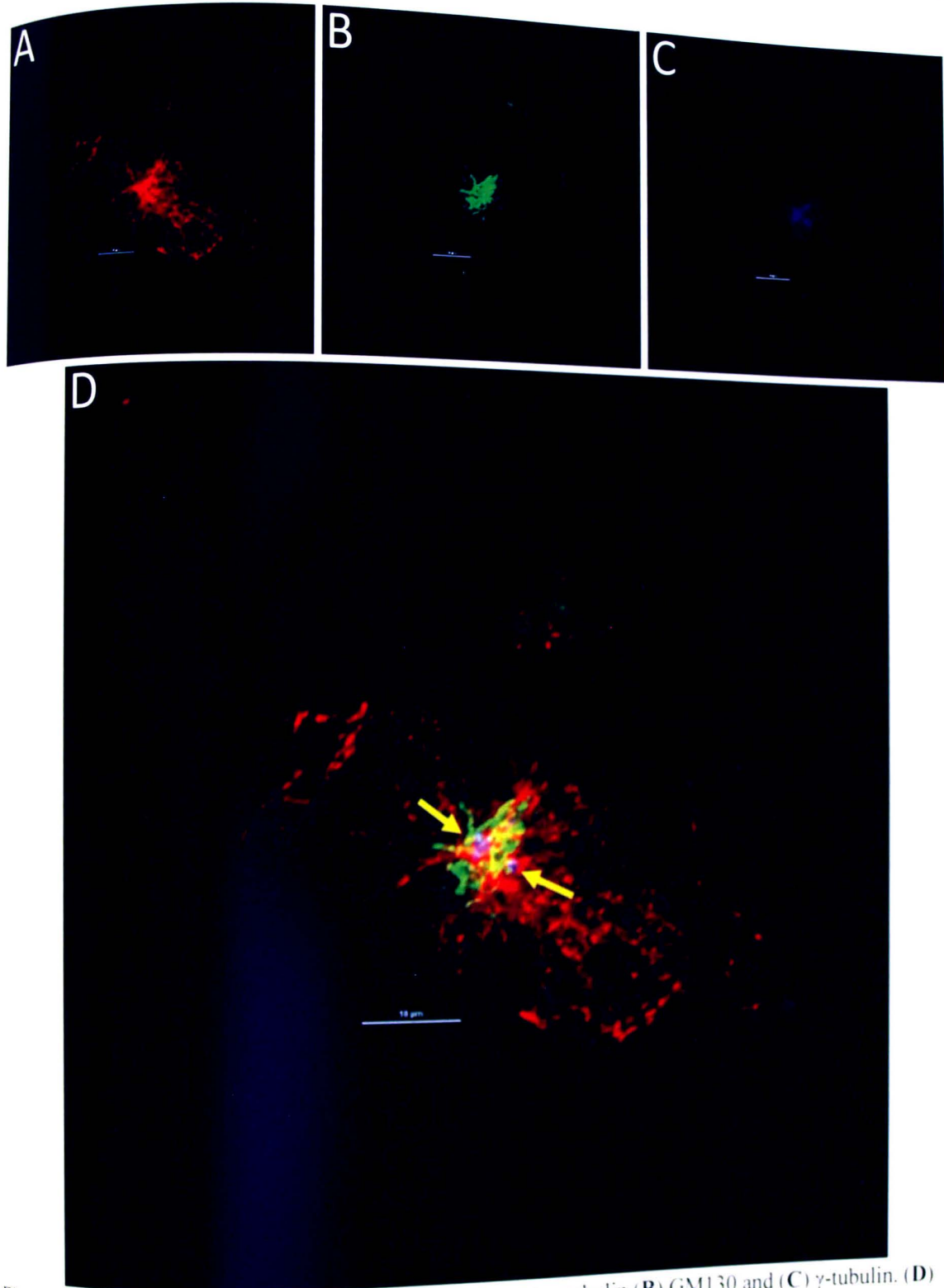


Figure 18. EGF-treated MDA-MB-231 cell stained for (A)  $\alpha$ -tubulin (B) GM130 and (C)  $\gamma$ -tubulin. (D) Merge of A-C shows more overlap between the blue  $\gamma$ -tubulin and the green Golgi. Scale bar represents 10  $\mu\text{m}$ .

## Colocalization for Migration Experiments

Z-stacks from ten fields of view were analyzed for colocalization for each cell group. The group mean and standard deviation for each of the four color/protein combinations can be seen below in Table 3 and Table 4. T-tests were used to compare controls to EGF-treated for each cell type. The appropriate one-way ANOVA was then used to compare all groups (Figures 19-22).









Mander's CC Mean $\pm$ STD	$\alpha$ -tubulin coloc GM130 $\alpha$ -tubulin	GM130 coloc $\alpha$ -tubulin GM130	GM130 coloc $\gamma$ -tubulin GM130	$\gamma$ -tubulin coloc GM130 $\gamma$ -tubulin
MCF-7 Control (n=10)	0.02 $\pm$ 0.01 	0.39 $\pm$ 0.16 	0.17 $\pm$ 0.08 	0.03 $\pm$ 0.02 
MCF-7 EGF-treated (n=10)	0.06 $\pm$ 0.04 t= 3.344 P<0.0069* 	0.60 $\pm$ 0.17 t= 2.869 P<0.0102* 	0.09 $\pm$ 0.08 t= -2.088 P=0.0513 	0.10 $\pm$ 0.06 t= 4.064 P<0.0021* 

Table 3. Colocalization summary table for MCF-7 EGF-induced migration. Summary table showing mean Mander's Colocalization Coefficient and standard deviation results. Groups were tested for equal variances using Levene's test. The appropriate t-test was then used (assuming equal variances or assuming unequal variances) to compare group means. Within each column, groups with different shapes are significantly different from one another, while those with the same shape are not. Significant p-values are in red.









Mander's CC Mean $\pm$ STD	$\alpha$ -tubulin coloc GM130 $\alpha$ -tubulin	GM130 coloc $\alpha$ -tubulin GM130	GM130 coloc $\gamma$ -tubulin GM130	$\gamma$ -tubulin coloc GM130 $\gamma$ -tubulin
MDA-MB-231 Control (n=10)	0.02 $\pm$ 0.01 	0.50 $\pm$ 0.14 	0.19 $\pm$ 0.10 	0.06 $\pm$ 0.04 
MDA-MB-231 EGF-treated (n=10)	0.20 $\pm$ 0.11 t=7.250 P<0.0001* 	0.89 $\pm$ 0.10 t=52.559 P<0.0001* 	0.15 $\pm$ 0.18 t= -0.537 P=0.5977 	0.47 $\pm$ 0.23 t=5.680 P<0.0003* 

Table 4. Colocalization summary table for MDA-MB-231 EGF-induced migration. Average Mander's Colocalization Coefficients and standard deviation results are shown for each color/protein combination. Groups were tested for equal variances using Levene's test. The appropriate t-test was then used (assuming equal variances or assuming unequal variances) to compare group means. Within each column, groups with different shapes are significantly different from one another, while those with the same shape are not. Significant p-values are in red.

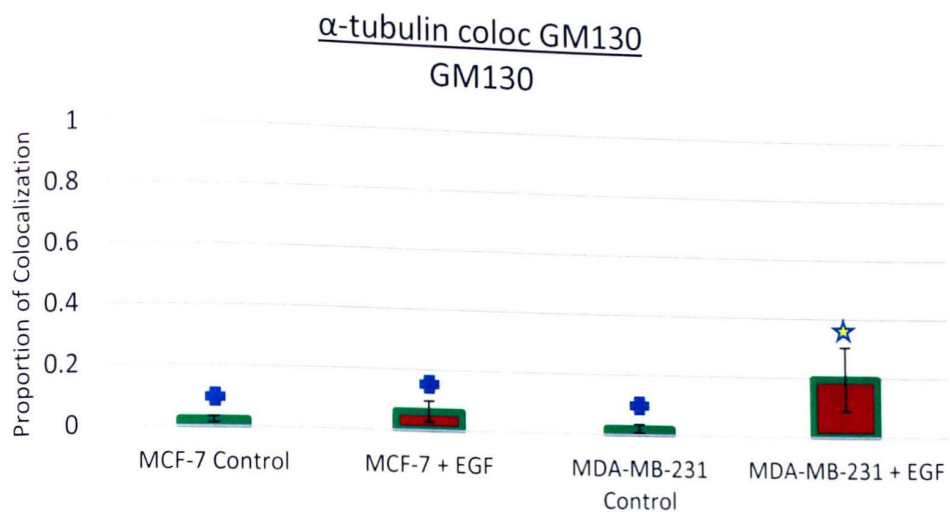


Figure 19. Bar graph showing the average proportion of  $\alpha$ -tubulin (red) colocalization with GM130 (green) for each cell group. Error bars reflect standard deviation. Levene's test indicates these groups have unequal variances so Welch's ANOVA and Tukey's post hoc test was used to compare group means. In this case, there is a significant difference between groups ( $F=11.389$ ,  $p<0.0002^*$ ). Groups with different shapes are significantly different from one another, while groups with the same shape are not. The EGF-treated MDA-MB-231 cells have a significantly higher colocalization value than the other three groups.

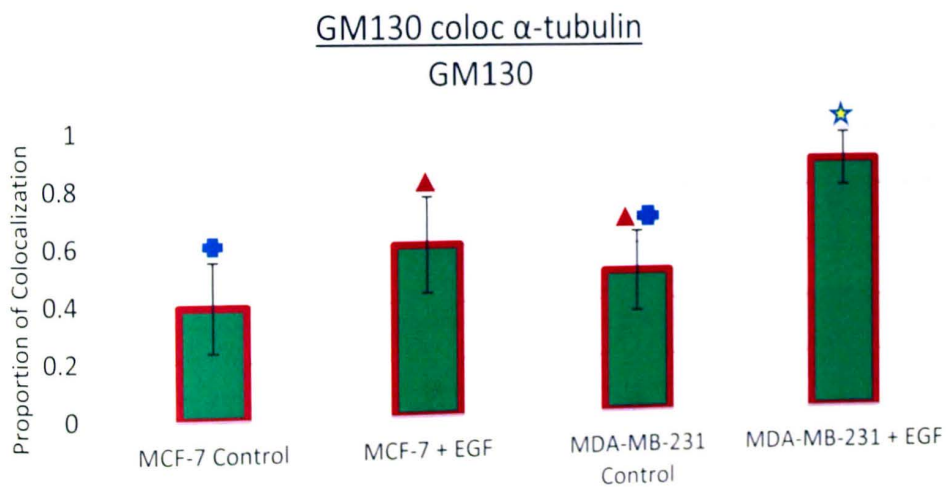


Figure 20. Average proportion of GM130 (green) colocalization with  $\alpha$ -tubulin (red) for each cell group. Error bars reflect standard deviation. Levene's test indicated these groups have equal variances so a one-way ANOVA and Tukey's post hoc test was used to compare group means. In this case, there was a significant difference between groups ( $F=22.260$ ,  $p<0.0001^*$ ). Groups with different shapes are significantly different from one another, while groups with the same shape are not. The EGF-treated MDA-MB-231 cells have a significantly higher colocalization value than the other three groups. The EGF-treated MCF-7 cells have a significantly higher colocalization value than the MCF-7 control cells, but not higher than the control MDA-MB-231 cells.

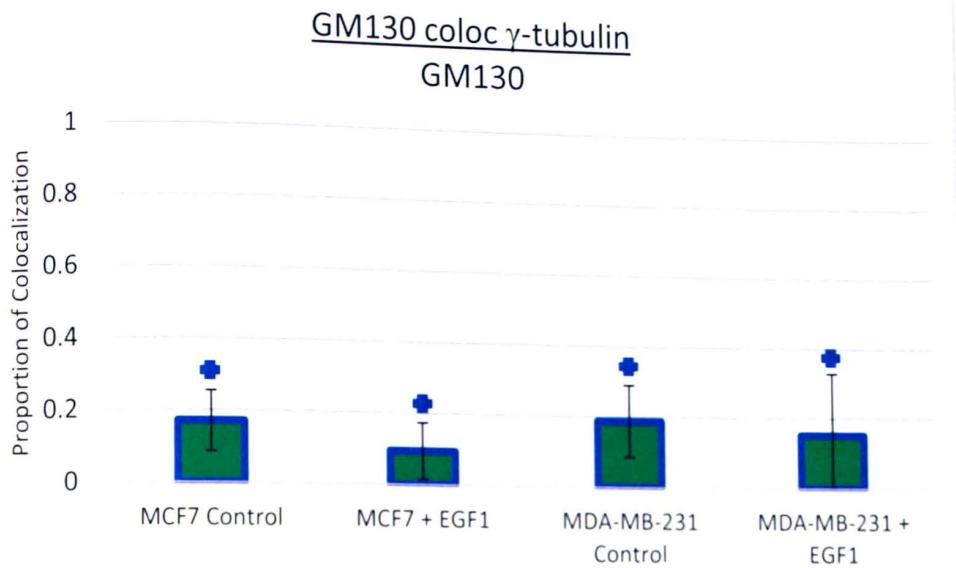


Figure 21. Average proportion of GM130 (green) colocalization with  $\gamma$ -tubulin (blue) for each cell group. Error bars reflect standard deviation. Levene's test indicated these groups have equal variances so group means were compared using a one-way ANOVA and Tukey's post hoc test. In this case, there was no significant difference between groups ( $F=1.2016$ ,  $p=0.3230$ ).

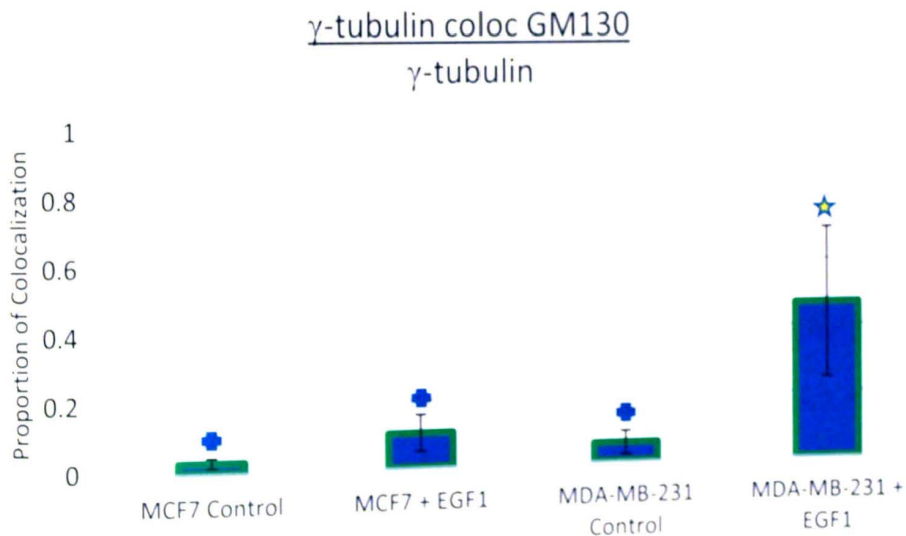


Figure 22. Average proportion of  $\gamma$ -tubulin (blue) colocalization with GM130 (green) for each cell group. Error bars reflect standard deviation. Levene's test indicated these groups have unequal variances so group means were compared using a Welch's ANOVA and Tukey's post hoc test. In this case, there was a significant difference between groups ( $F=17.062$ ,  $p<0.0001^*$ ). Groups with different shapes are significantly different from one another, while groups with the same shape are not. The EGF-treated MDA-MB-231 cells had a significantly higher colocalization value than the other three groups.

## Discussion and Conclusions

Golgi Distribution in MCF-7 Cells

In general, we found the Golgi apparatus to have a scattered distribution in MCF-7 cells, both control and treated. Rather than the perinuclear compact arrangement typically expected for animal cells, these cells appeared to have multiple mini-stacks randomly distributed throughout the cytoplasm. This observation supports a study published by Schindler *et al.* (1996) showing MCF-7 cells to have a dispersed, fragmented distribution of their *trans*-Golgi network (TGN) which they also found to be poorly acidified. These cells exhibit a low pH gradient between intravesicular compartments (pH 6.5) and the cytoplasm (pH 6.8), which Schindler *et al.* hypothesize is responsible for MCF-7 drug-sensitivity. In contrast, drug-resistant MCF-7<sup>adr</sup> cells, derived from the MCF-7 parental line, have a more typical perinuclear arrangement of their Golgi and exhibit a higher pH gradient between their TGN (pH 5.9) and the cytoplasm (pH 7.1). Treatment of the MCF-7<sup>adr</sup> cells with monensin, a sodium proton ionophore, causes an alkaline shift in the pH, lowering their pH gradient and increasing their drug sensitivity to that of the parental MCF-7 cell line, while also disrupting their Golgi distribution.

Kellokumpo *et al.* (2002) also reported a heavily fragmented and scattered Golgi in MCF-7 cells, as well as several colorectal cancer cell lines, and using transmission electron microscopy, found the cisternae of Golgi stacks in these cells to be severely dilated. This study proposes that Golgi structure is directly dependent upon Golgi pH, and also links that with abnormal glycosylation abilities. Defects in pH regulation of the Golgi have also been shown to interfere with polarized vesicle secretion (Caplan *et al.*, 1987). Precisely how pH could control Golgi structure is not known. As discussed in the introduction though, Hurtado *et al.* (2011)

found that Golgi-derived MTs play a critical role in maintaining overall Golgi structure, and thus it is possible that lack of this subset of MTs could also play a role in the scattered Golgi distribution found in MCF-7 cells.

### Microtubule Disassembly

Our experiments found MTs in MCF-7 cells to be more resistant to experimental manipulations aimed at disassembly than those in MDA-MB-231 cells. Microtubules in MDA-MB-231 cells were readily disassembled by 40 minutes of ice incubation or four hours of nocodazole treatment, but these same approaches left many MTs intact in MCF-7 cells. Nocodazole is widely used in MT studies because it binds with high affinity to tubulin, effectively blocking MT assembly, while MT disassembly continues to occur (Xu *et al.*, 2002). Abrupt cooling to 4°C has also been repeatedly shown to experimentally depolymerize MTs in many cell types, likely due to a change in reaction kinetics that inhibit assembly and promote disassembly (Fygenson *et al.*, 1994; Karr *et al.*, 1980). However, animals that regularly survive at cold temperatures, such as Antarctic fishes, exhibit cold-tolerant MTs capable of assembling at temperatures as low as 5-20°C, albeit a bit slower than at 37°C (Detrich, 1997). This tolerance to cold surely offered these species an evolutionary advantage, but cold-stable microtubules have also been found in mammalian neurons, peripheral nerves, and fibroblasts that did not follow this same pattern of development (Webb and Wilson, 1980; Oka *et al.*, 1994; Bershadsky *et al.*, 1979). Likewise, many of these same cell types also display resistance to nocodazole treatment, similar to the MCF-7 cells in our experiments.

Several mechanisms could be responsible for the enhanced stability of certain MTs. Some studies have shown that stable MTs exhibit more post-translational modifications, including acetylation and detyrosination, but these changes are not thought to confer stability

directly (Khawaja *et al.*, 1988; Quinones *et al.*, 2011). Instead, they likely serve to help mediate the interaction of MTs with microtubule-associated proteins (MAPs), which do play a more direct role in MT stability. For example, the MAP tau, which is particularly abundant in neurons, has been shown to protect MTs against nocodazole exposure, even when introduced into cells that are not normally nocodazole-resistant (Lee and Rook, 1992). However, this protein does not protect MTs against cold treatment (Baas *et al.*, 1994). Instead, a MAP protein called stable tubule-only polypeptide (STOP) isolated from brain tissue, has been shown to bind to MTs and stabilize them against cold temperatures (Margolis *et al.*, 1990). Isoforms of this protein have also been found in mammalian fibroblasts, where they exert the same effect (Denarier *et al.*, 1998). Furthermore, introduction of this protein into HeLa cells induces cold stability of their MTs, which normally depolymerize rapidly when exposed to cold temperatures (0°C). Given that our MCF-7 cells required both nocodazole and cold treatment to completely depolymerize MTs, there is likely more than one stabilizing mechanism at play here.

### MT Nucleation at the Golgi

The first objective of this thesis research was to look for evidence of MT nucleation at the Golgi in breast cancer cells with different migratory potentials. Given that Golgi-derived MTs are critical for directed cell migration, this work was done with the hypothesis that the invasive MDA-MB-231 cells would exhibit MTs originating from the Golgi while the MCF-7 cells would not. Depolymerizing MTs and allowing brief regrowth allowed for better detection of nucleation events that would otherwise be obscured by the full MT network. Though not present in every cell, instances of overlap between the *cis*-Golgi marker GM130,  $\alpha$ -tubulin, and EB1 could be seen more frequently in both the ice-treated and nocodazole-treated MDA-MB-231 cells as

compared to the MCF-7. Though the goal was to see newly growing MTs individually, this proved not entirely possible with the 60x objective. Higher magnification with better resolution would surely benefit this endeavor. Nonetheless, using the more impartial method of quantitative colocalization analysis revealed values that, when taken together, support the original hypothesis. It was very difficult to achieve exactly the same amount of regrowth in various plates of cells, and thus differences in relative amounts of  $\alpha$ -tubulin would have an impact on some of these numbers. For example, the average amount of  $\alpha$ -tubulin colocalized with GM130 relative to the total amount of  $\alpha$ -tubulin present was lower in the ice-treated MDA-MB-231 cells than the nocodazole-treated cells. This is because the individual MTs recovered more quickly from ice treatment, and since they were longer in length there was a greater amount of red present. However, one would not expect the amount of red colocalizing with green to go up proportionally in this case because it is really only the minus ends of MTs that should exhibit this overlap. Ideally, to make these comparisons between cell groups, it would be best to have exactly the same amount of MT regrowth across cells. These experiments were repeated a number of times in the attempt to achieve that goal, but ultimately time and resources became limitations.

The second objective of this thesis research was to determine if MT nucleation at the Golgi is more apparent during active migration in response to the chemoattractant EGF compared to untreated cells. This was done by looking for colocalizations between the Golgi,  $\alpha$ -tubulin, and  $\gamma$ -tubulin, with the hypothesis that colocalization values would be higher in EGF-treated cells versus controls. Qualitative evaluation of the images found some  $\gamma$ -tubulin dispersed faintly within the cytoplasm of all cells, but prominent staining existed in generally one localized spot for MCF-7 cells, as expected for the centrosome. This typical centrosomal staining also appeared in many MDA-MB-231 cells. However, some EGF-treated MDA-MB-231 cells

displayed multiple concentrated spots of  $\gamma$ -tubulin, which also colocalized with the Golgi (Figure 18). Quantitative analysis revealed significantly higher values in three out of the four protein/color combinations for EGF-treated MDA-MB-231 cells compared to controls. This was also true for EGF-treated MCF-7 cells, albeit the overall values were much lower in these cells. Comparing all groups together found only the EGF-treated MDA-MB-231 cells to be significantly different from the other three cell groups. Given that most EGF-treated MCF-7 cells never took on the typical polarized morphology indicative of directed migration, it is not surprising that their colocalization values were not as high as those for the EGF-treated MDA-MB-231 cells. Plating MCF-7 cells on fibronectin, though, could help improve their migratory ability. Overall, the results of this thesis work provide evidence in support of the hypothesis that highly migratory cells such as MDA-MB-231 line nucleate MTs from the Golgi more frequently than in cells exhibiting less migratory potential.

### Future Implications

Finding the presence of MT nucleation at the Golgi in invasive cancer cell types could have implications for developing new drug therapies to potentially limit metastasis. Given the proliferative nature of cancer cells and the essential role MTs play in that process, they are an obvious target of choice for most prevalently used chemotherapeutic drugs available (Pasquier and Kavallaris, 2008). However, these drugs target all MTs indiscriminately, and thus can have negative side effects, including neuropathy, myelosuppression, and mucositis, associated with damage to non-cancer cells that normally divide rapidly. Other studies have shown that Golgi-derived MTs can be inhibited specifically, while leaving centrosomal MTs intact, by blocking the proteins CLASPs, GCC185, or AKAP450 (Efimov *et al.*, 2007; Hurtado *et al.*, 2011). If this knowledge can be used to develop therapies for patients, it could potentially slow metastatic

spread of particularly invasive cancers. In theory, this type of treatment would not stop these cancers from proliferating, but could slow their ability to invade other tissues in a directed sense. However, cells that display directed migration normally, such as those of the immune system, could be unintended targets of these therapies. To know if this is a feasible route of inquiry, the presence or absence of Golgi-derived MTs needs to be established in more cell types, including both cancer and non-cancer cells.

### Conclusions

In conclusion, this study shows that the highly invasive MDA-MB-231 cell line has significantly more microtubule nucleation events at the Golgi than do the less invasive MCF-7 cell line. The ability of the Golgi apparatus to nucleate MTs independent of the centrosome is an important discovery in basic cell function. Generating unique subsets of MTs enables a cell to establish arrays capable of fulfilling distinct tasks, which would be particularly useful for the highly coordinated and complicated process of cell migration. Finding evidence of significantly greater numbers of Golgi-derived MTs in the highly migratory MDA-MB-231 breast cancer cells as compared to the weakly migratory MCF-7 cells provides an important distinction related to their invasive potential.

## LITERATURE CITED

- Alberts B, Johnson A, Lewis J, Raff M, Roberts K, and Walter P. Molecular Biology of the Cell. New York: Garland Science; 2002.
- Ali S and Coombes RC. Estrogen receptor alpha in human breast cancer: occurrence and significance. *Journal of Mammary Gland Biology and Neoplasia*, 2000; 5(3): 271-281.
- Baas PW, Pienkowski TP, Cimbalnik KA, Toyama K, Bakalis S, Ahmad FJ, and Kosik KS. Tau confers drug stability but not cold stability to microtubules in living cells. *Journal of Cell Science*, 1994; 107: 135-143.
- Bershadsky AD, Gelfand VI, Svitkina TM, and Tint IS. Cold-stable microtubules in the cytoplasm of mouse embryo fibroblasts. *Cell Biology International Reports*, 1979; 3(1): 45-50.
- Bisbal M, Wojnacki J, Peretti D, Ropolo A, Sesma J, Jausoro I, and Cáceres A. KIF4 mediates anterograde translocation and positioning of ribosomal constituents to axons. *The Journal of Biological Chemistry*, 2009; 284(14): 9489-9497.
- Bolte S and Cordelières FP. A guided tour into subcellular colocalization analysis in light microscopy. *Journal of Microscopy*, 2006; 224, Pt 3: 213-232.
- Bozzuto G, Condello M, and Molinari A. Migratory behavior of tumour cells: a scanning electron microscopy study. *Annali dell'Istituto Superiore di Sanità*, 2015; 51(2): 139-147.
- Bracker CE, Grove SN, Heintz CE, and Morre DJ. Continuity between endomembrane components in hyphae of *Pythium* spp. *Cytobiologie*, 1971; 4: 1-8.
- Bretcher MS and Aguado-Velasco C. Membrane traffic during cell locomotion. *Current Opinions in Cell Biology*, 1998; 10(4): 537-541.
- Cailleau R, Olivé M, and Cruciger QVJ. Long-term human breast carcinoma cell lines of

metastatic origin: preliminary characterization. *In Vitro*, 1978; 14(11): 911-915.

Caplan MJ, Stow JL, Newman AP, Madri J, Anderson HC, Farquhar MG, Palade GE, and Jamieson JD. Dependence on pH of polarized sorting of secreted proteins. *Nature*, 1987; 329: 632-635.

Carlier MF, Didry D, and Pantaloni D. Hydrolysis of GTP associated with the formation of tubulin oligomers is involved in microtubule nucleation. *Biophysical Journal*, 1997; 73: 418-427.

Chabin-Brion K, Marceiller J, Perez F, Settegrana C, Drechou A, Durand G, Pous C. The Golgi complex is a microtubule-organizing organelle. *Molecular Biology of the Cell*, 2001; 12: 2047-2060.

Chavez KJ, Garimella SV, Lipkowitz S. Triple negative breast cancer cell lines: one tool in the search for better treatment of triple negative breast cancer. *Breast Disease*, 2010; 32(1-2): 35-48.

Chen J-Q and Russo J. ER $\alpha$ -negative and triple negative breast cancer: molecular features and potential therapeutic approaches. *Biochimica et biophysica acta*, 2009; 1796(2): 162-175.

Cluett EB and Brown WJ. Adhesion of Golgi cisternae by proteinaceous interactions: intercisternal bridges as putative adhesive structures. *Journal of Cell Science*, 1992; 103: 773-784.

Cole NB, Sciaky N, Marotta A, Song J, and Lippincott-Schwartz J. Golgi dispersal during microtubule disruption: regeneration of Golgi stacks at peripheral endoplasmic reticulum exit sites. *Molecular Biology of the Cell*, 1996; 7(4): 631-50.

- De Bruyne GK, Bracke ME, Plessers L, and Mareel MM. Invasiveness in vitro of mixed aggregates composed of two human mammary cell lines MCF-7 and HBL-100. *Invasion Metastasis*, 1988; 8(5): 253-265.
- Delphin C, Bouvier D, Seggio M, Couriol E, Saoudi Y, Denarier E, Bose C, Valiron O, Bisbal M, Arnal I, and Andrieux A. MAP6-F is a temperature sensor that directly binds to and protects microtubules from cold-induced depolymerization. *Journal of Biological Chemistry*, 2012; 287(42): 35127-35138.
- Detrich, HW. Microtubule assembly in cold-adapted organisms: functional properties and structural adaptations of tubulins from Antarctic fishes. *Comparative Biochemistry and Physiology, Part A: Physiology*, 1997; 118(3): 501-513.
- Dong C, Slattery M, and Liang S. Micromechanics of tumor cell adhesion and migration under dynamic flow conditions. *Frontiers in Bioscience*, 2005; 10: 379-384.
- Efimov A, Kharitonov A, Efimova N, Loncarek J, Miller PM, Andreyeva N, Gleeson P, Galjart N, Maia A, McLeod IX, Yates JR, Maiato H, Khodjakov A, Akhmanova A, and Kaverina I. Asymmetric CLASP-dependent nucleation of non-centrosomal microtubules at the trans-Golgi network. *Developmental Cell*, 2007; 12(6): 917-930.
- Etienne-Manneville S. Microtubules in cell migration. *Annual Review of Cell and Developmental Biology*, 2013; 29: 471-499.
- Feldman JL and Priess JR. A role for the centrosome and PAR3 in the hand-off of microtubule organizing function during epithelial polarization. *Current Biology*, 2012; 22(7): 575-582.
- Friedman JR, Webster BM, Mastronarde DN, Verhey KJ, and Voeltz GK. ER sliding dynamics and ER-mitochondrial contacts occur on acetylated microtubules. *Journal of Cell Biology*, 2010; 190(3): 363-375.

- Fygenon, DK, Braun E, and Libchaber A. Phase diagram of microtubules. *Physical Review. E, Statistical physics, plasmas, fluids, and related interdisciplinary topics*, 1994; 50(2): 1579-1588.
- Grimaldi AD, Fomicheva M, and Kaverina I. Ice recovery assay for detection of Golgi-derived microtubules. *Methods in Cell Biology*, 2013; 118: 401-415.
- Ho WC, Allan VJ, van Meer G, Berger EG, and Kreis TE. Reclustering of scattered Golgi elements occurs along microtubules. *European Journal of Cell Biology*, 1989; 48(2): 250-263.
- Holliday DL and Speirs V. Choosing the right cell line for breast cancer research. *Breast Cancer Research*, 2011; 13(4): 215.
- Horio T. and Murata T. The role of dynamic instability in microtubule organization. *Front Plant Sci*, 2014; 5(511).
- Howlader N, Noone AM, Krapcho M, Miller D, Bishop K, Altekruse SF, Kosary CL, Yu M, Ruhl J, Tatalovich Z, Mariotto A, Lewis DR, Chen HS, Feuer EJ, Cronin KA (eds). SEER Cancer Statistics Review, 1975-2013, National Cancer Institute. Bethesda, MD, [http://seer.cancer.gov/csr/1975\\_2013/](http://seer.cancer.gov/csr/1975_2013/), based on November 2015 SEER data submission, posted to the SEER web site, April 2016. Accessed April 17, 2016.
- Hua Z, Graham TR. The Golgi Apparatus. In: Madame Curie Bioscience Database [Internet]. Austin (TX): Landes Bioscience; 2000-2013. Available from: <http://www.ncbi.nlm.nih.gov/books/NBK6268/>
- Hunter KW, Crawford NPS, Alsarraj J. Mechanisms of metastasis. *Breast Cancer Research*, 2008; 10(Suppl 1): S2.
- Hurtado L, Caballero C, Gavilan MP, Cardenas J, Bornens M, and Rios RM. Disconnecting the

Golgi ribbon from the centrosome prevents directional cell migration and ciliogenesis. *Journal of Cell Biology*, 2011; 193(5): 917-933.

International Agency for Research on Cancer (IARC) and World Health Organization (WHO).

GLOBOCAN 2012: Estimated cancer incidence, mortality and prevalence worldwide in 2012. [http://globocan.iarc.fr/Pages/fact\\_sheets\\_cancer.aspx](http://globocan.iarc.fr/Pages/fact_sheets_cancer.aspx), 2016. Accessed April 17, 2016.

Karr TL, Kristofferson D, and Purich DL. Mechanism of microtubule depolymerization: a reevaluation of cold-induced microtubule depolymerization kinetics by employing a rapid heat exchanger method. *Journal of Biological Chemistry*, 1980; 225(18): 8560-8566.

Kaverina I, Krylyshkina O, and Small JV. Microtubule targeting of substrate contacts promotes their relaxation and dissociation. *Journal of Cell Biology*, 1999; 146: 1033-1044.

Keating TJ and Borisy GG. Immunostuctural evidence for the template mechanism of microtubule nucleation. *Nature Cell Biology*, 2000; 2(6): 352-7.

Kellokumpu S, Sormunen R, and Kellokumpu I. Abnormal glycosylation and altered Golgi structure in colorectal cancer: dependence on intra-Golgi pH. *FEBS Letters*, 2002; 516(1-3): 217-224.

Khajah MA, Saleh SA, Mathew PM, and Luqmani YA. Differential effect of growth factors on invasion and proliferation of endocrine resistant breast cancer cells. *PLoS One*, 2012; 7(7): e41847.

Khawaja S, Gunderson GG, and Bulinski JC. Enhanced stability of microtubules enriched in detyrosinated tubulin is not a direct function of detyrosination level. *Journal of Cell Biology*, 1988; 106: 141-149.

Kim BJ, Hannanta-anan P, Chau M, Kim YS, Swartz MA, and Wu M. Cooperative roles of SDF-1 $\alpha$  and EGF gradients on tumor cell migration revealed by a robust 3D microfluidic

model. *PLoS ONE*, 2013; 8(7): e68422.

Kobayashi T and Dynlacht BD. Regulating the transition from centriole to basal body. *Journal of Cell Biology*, 2011; 193(3): 435-444.

Kollman JM, Merdes A, Mourey L, and Agard DA. Microtubule nucleation by  $\gamma$ -tubulin complexes. *Nature Reviews Molecular Cell Biology*, 2011; 12: 709-721.

Krendel M, Zenke FT, and Bokoch GM. Nucleotide exchange factor GEF-H1 mediates crosstalk between microtubules and the actin cytoskeleton. *Nature Cell Biology*, 2002; 4: 294-301.

Lee AV, Oesterreich S, and Davidson NE. MCF-7 cells—changing the course of breast cancer research and care for 45 years. *Journal of the National Cancer Institute*, 2015; 107(7): djv073.

Lee G, and Rook SL. Expression of tau protein in non-neuronal cells: microtubule binding and stabilization. *Journal of Cell Science*, 1992; 102: 227-237.

Lippincott-Schwartz J, Cole NB, Marotta A, Conrad PA, and Bloom GS. Kinesin is the motor for microtubule-mediated Golgi-to-ER membrane traffic. *The Journal of Cell Biology*, 1995; 128(3): 293-306.

Malikov V, Kashina A, and Rodionov V. Cytoplasmic dynein nucleates microtubules to organize them into radial arrays in vivo. *Molecular Biology of the Cell*, 2004; 15(6): 2742-2749.

Margolis RL, Rauch CT, Pirollet F, and Job D. Specific association of STOP protein with microtubules in vitro and with stable microtubules in mitotic spindles of cultured cells. *European Molecular Biology Organization (EMBO) Journal*, 1990; 9(12): 4095-4102.

Mingle LA, Okuhama NN, Shi J, Singer RH, Condeelis J, and Liu G. Localization of all seven messenger RNAs for the actin-polymerizing nucleator Arp2/3 complex in the protrusions of fibroblasts. *Journal of Cell Science*, 2005; 118: 2425-2433.

- Miller PM, Folkmann AW, Maia ARR, Efimova N, Efimov A, and Kaverina, I. Golgi-derived CLASP-dependent microtubules control Golgi organization and polarized trafficking in motile cells. *Nature Cell Biology*, 2009; 11(9): 1069-1080.
- Mitchell DR. The evolution of eukaryotic cilia and flagella as motile and sensory organelles. *Advances in Experimental Medicine and Biology*, 2007; 607: 130-140.
- Moritz M, Braunfeld MB, Sedat JW, Alberts B, Agard DA. Microtubule nucleation by  $\gamma$ -tubulin-containing rings in the centrosome. *Nature*, 1995; 378: 638–640.
- Moritz M, Braunfeld MB, Guenebaut V, Heuser J, and Agard, DA. Structure of the  $\gamma$ -tubulin ring complex: a template for microtubule nucleation. *Nature Cell Biology*, 2000; 2: 365-370.
- Mukherjee D and Zhao J. The role of chemokine receptor CXCR4 in breast cancer metastasis. *American Journal of Cancer Research*, 2013; 3(1): 46-57.
- Muller A, Homey B, Soto H, Ge N, Catron D, Buchanan ME, McClanahan T, Murphy E, Yuan W, Wagner SN, Barrera JL, Mohar A, Verastegui E, and Zlotnik A. Involvement of chemokine receptors in breast cancer metastasis. *Nature*, 2001; 410: 50-56.
- Murata T, Sonobe S, Baskin TI, Hyodo S, Hasezawa S, Nagata T, Horio T, and Hasebe M. Microtubule-dependent microtubule nucleation based on recruitment of gamma-tubulin in higher plants. *Nature Cell Biology*, 2005; 7(10): 961-968.
- Murphy SM, Urbani L, and Stearns T. The mammalian  $\gamma$ -tubulin complex contains homologues of the yeast spindle pole body components Spc97p and Spc98p. *The Journal of Cell Biology*, 1998; 141(3): 663-674.
- Nelson MT, Short A, Cole SL, Gross AC, Winter J, Eubank TD, and Lannutti JJ. Preferential, enhanced breast cancer cell migration on biomimetic electrospun nanofiber 'cell highways'. *BioMed Central Cancer*, 2014; 14: 825.

- Nieman MT, Prudoff RS, Johnson KR, and Wheelock MJ. N-Cadherin promotes motility in human breast cancer cells regardless of their E-cadherin expression. *The Journal of Cell Biology*, 1999; 147(3): 631-644.
- Oddoux S, Zaal KJ, Tate V, Kenea A, Nandkeolyar SA, Reid E, Liu W, and Ralston E. Microtubules that form the stationary lattice of muscle fibers are dynamic and nucleated at Golgi elements. *Journal of Cell Biology*, 2013; 203: 205-213.
- Oegema K, Wiese C, Martin OC, Milligan RA, Iwamatsu A, Mitchison TJ, and Zheng Y. Characterization of two related *Drosophila*  $\gamma$ -tubulin complexes that differ in their ability to nucleate microtubules. *Journal of Cell Biology*, 1999; 144(4): 721-733.
- Oka N, Nishio T, Akiguchi I, Nagao M, Kawasaki T, and Kimura J. Microtubules stability in human peripheral nerves. *Neuroscience Letters*, 1994; 168(1-2): 61-64.
- Pasquier E and Kavallaris M. Microtubules: a dynamic target in cancer therapy. *IUBMB Life*, 2008; 60(3): 165-170.
- Patsialou A, Wyckoff J, Wang Y, Goswami S, Stanley ER, and Condeelis JS. Invasion of human breast cancer cells in vivo requires both paracrine and autocrine loops involving the colony stimulating factor-1 receptor. *Cancer Research*. 2009; 69(24): 9498-9506.
- Picone R, Ren X, Ivanovitch KD, Clarke JDW, McKendry RA, and Baum B. A polarised population of dynamic microtubules mediates homeostatic length control in animal cells. Mogilner A, ed. *PLoS Biology*, 2010; 8(11): e1000542.
- Price JT, Tiganis T, Agarwal A, Djakiew D, and Thompson EW. Epidermal growth factor promotes MDA-MB-231 breast cancer cell migration through a phosphatidylinositol 3'-kinase and phospholipase C-dependent mechanism. *Cancer Research*, 1999; 59: 5475-5478.

- Quinones GB, Danowski BA, Devaraj A, Singh V, and Ligon LA. The posttranslational modification of tubulin undergoes a switch from detyrosination to acetylation as epithelial cells become polarized. *Molecular Biology of the Cell*, 2011; 22(7): 1045-1057.
- Rasband, WS, ImageJ, U. S. National Institutes of Health, Bethesda, Maryland, USA, <http://imagej.nih.gov/ij/>, 1997-2015
- Rogalski AA and Singer SJ. Associations of elements of the Golgi apparatus with microtubules. *Journal of Cell Biology*, 1984; 99: 1092-1100.
- Schindler M, Grabski S, Hoff E, and Simon SM. Defective pH regulation of acidic compartments in human breast cancer cells (MCF-7) is normalized in adriamycin-resistant cells (MCF-7adr). *Biochemistry*, 1996; 35(9): 2811-2817.
- Schmit AC. Acentrosomal microtubule nucleation in higher plants. *International Review of Cytology*, 2002; 220: 257-289.
- Soule HD, Vazquez J, Long A, Albert S, and Brennan M. A human cell line from a pleural effusion derived from a breast carcinoma. *Journal of the National Cancer Institute*, 1973; 51(5): 1409-1416.
- Stehbens S and Wittmann T. Targeting and transport: how microtubules control focal adhesion dynamics. *Journal of Cell Biology*, 2012; 198(4): 481-489.
- Stoletov K, Kato H, Zardouzian E, Kelber J, Yang J, Shattil S, and Klemke R. Visualizing extravasation dynamics of metastatic tumor cells. *Journal of Cell Science*, 2010; 123: 2332-2341.
- Sun R, Gao P, Chen L, Ma D, Wang J, Oppenheim JJ, and Zhang N. Protein Kinase C is required for epidermal growth factor-induced chemotaxis of human breast cancer cells. *Cancer Research*, 2005; 65: 1433.

- Tanaka K, Mitsushima A, Fukudome H, and Kashima Y. Three-dimensional architecture of the Golgi complex observed by high resolution scanning electron microscopy. *Journal of Submicroscopic Cytology and Pathology*, 1986; 18: 1-9.
- Vogel JM, Stearns T, Rieder CL, Palazzo RE. Centrosomes isolated from *Spisula solidissima* oocytes contain rings and an unusual stoichiometric ratio of  $\alpha/\beta$  tubulin. *Journal of Cell Biology*, 1997; 137: 193–202.
- Voldborg BR, Damstrup L, Spang-Thomsen M, and Poulsen HS. Epidermal growth factor receptor (EGFR) and EGFR mutations, function, and possible role in clinical trials. *Annals of Oncology*, 1997; 8: 1197-1206.
- Webb BC and Wilson L. Cold-stable microtubules from brain. *Biochemistry*, 1980; 19: 1993-2001.
- Xu K, Schwarz PM, and Luduena RF. Interaction of nocodazole with tubulin isotypes. *Drug Development Research*, 2002; 55(2): 91-96.
- Zhai Y and Borisy G. Quantitative determination of the proportion of microtubule polymer present during the mitosis-interphase transition. *Journal of Cell Science*, 1994; 107: 881-890.
- Zheng Y, Wong ML, Alberts B, and Mitchison T. Nucleation of microtubule assembly by a  $\gamma$ -tubulin-containing ring complex. *Nature*, 1995; 378: 578–583.
- Zhu X and Kaverina I. Quantification of asymmetric microtubules nucleation at sub-cellular structures. *Methods in Molecular Biology*, 2011; 777: 235-244.

## APPENDIX A: Photographs

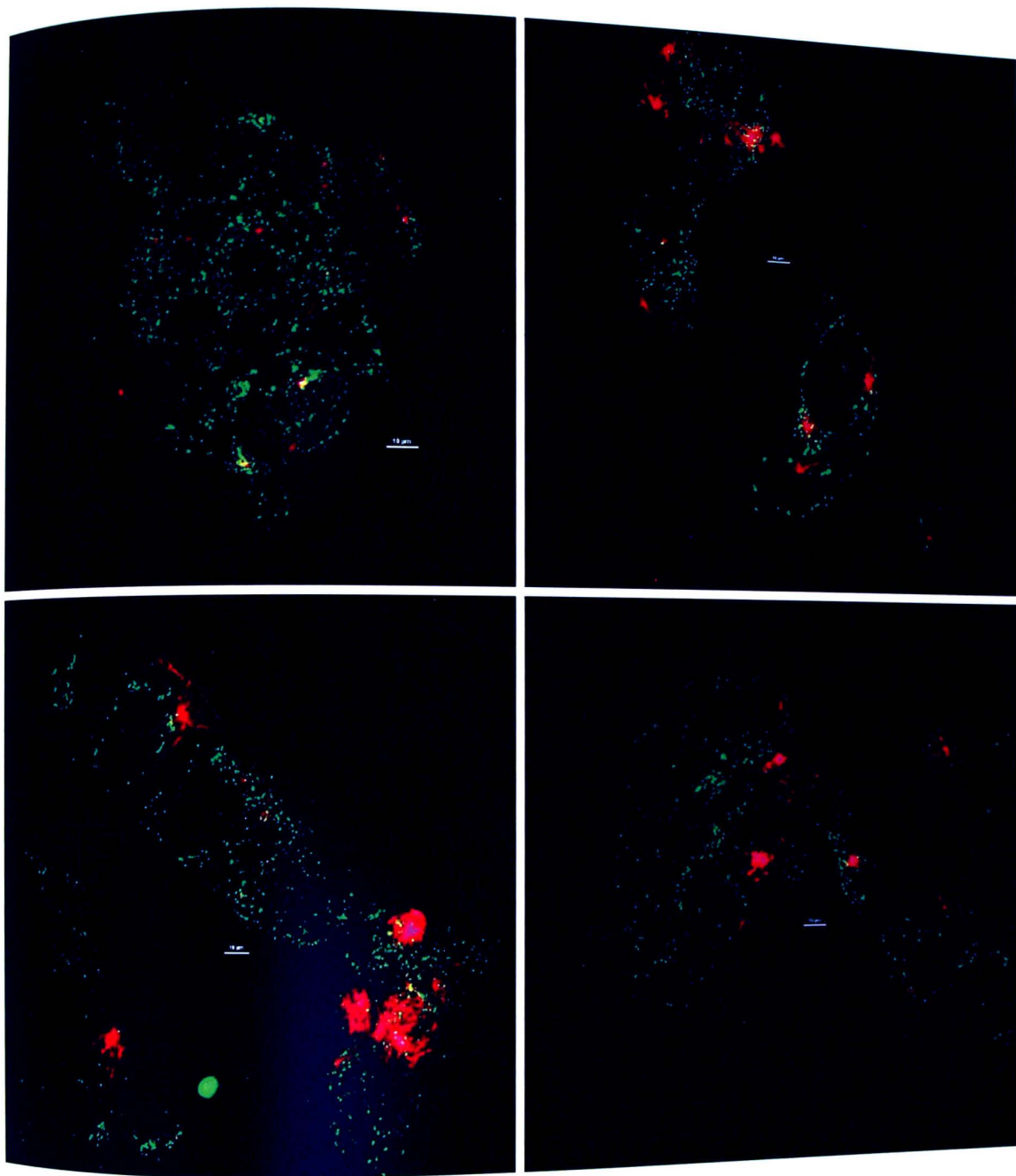


Figure 23. Additional images of MT regrowth in MCF-7 cells following 5h nocodazole + 30m ice + 4m regrowth. In addition to the image seen in figure 7, these are the four other fields of view that were analyzed for colocalization. These are max intensity images of z-stacks, and thus not all of the overlap that appears here was actually within the same focal plane. Scale bar represents 10μm.

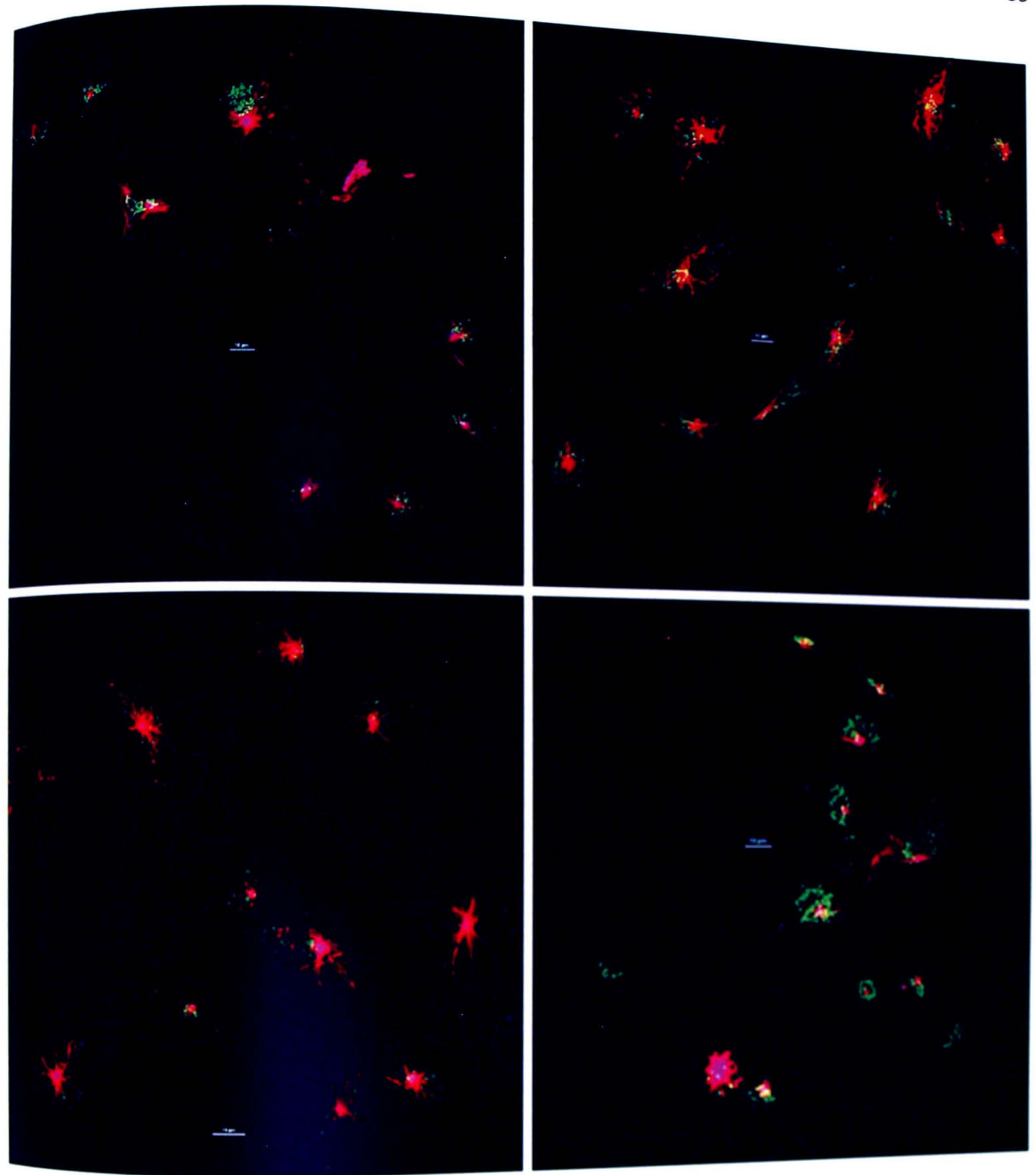


Figure 24. Additional images of MT regrowth in MDA-MB-231 cells following 40m ice + 40s regrowth. In addition to the image seen in figure 9, these are the four other fields of view that were analyzed for colocalization. These are max intensity images of z-stacks, and much of the color overlap seen here was also present within the same focal plane. Scale bar represents 10 $\mu$ m.

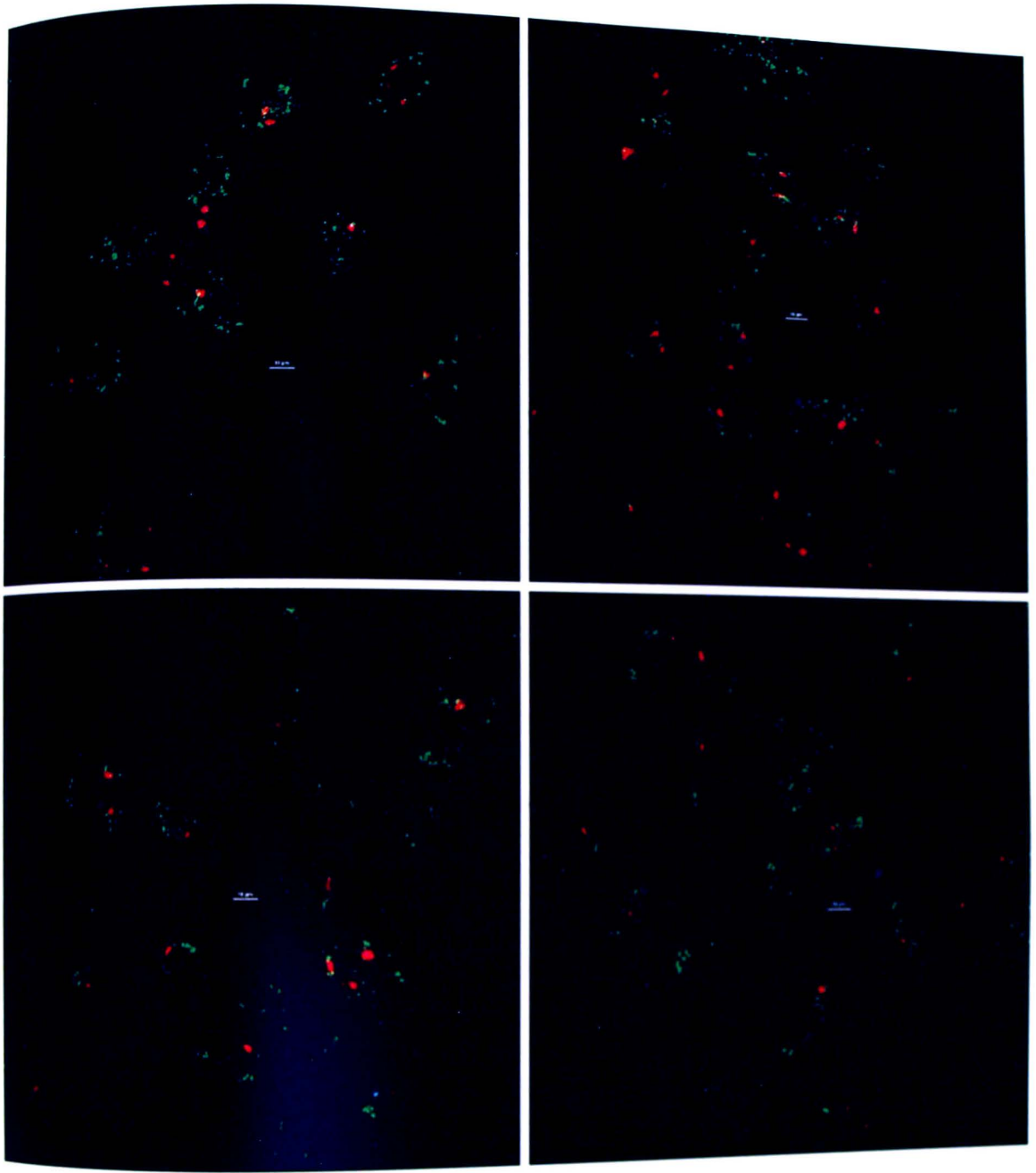


Figure 25. Additional images of MT regrowth in MDA-MB-231 cells following 4h nocodazole + 60s regrowth. In addition to the image seen in figure 10, these are the four other fields of view that were analyzed for colocalization. These are max intensity images of z-stacks, and much of the color overlap seen here was also present within the same focal plane. Scale bar represents 10 $\mu$ m.

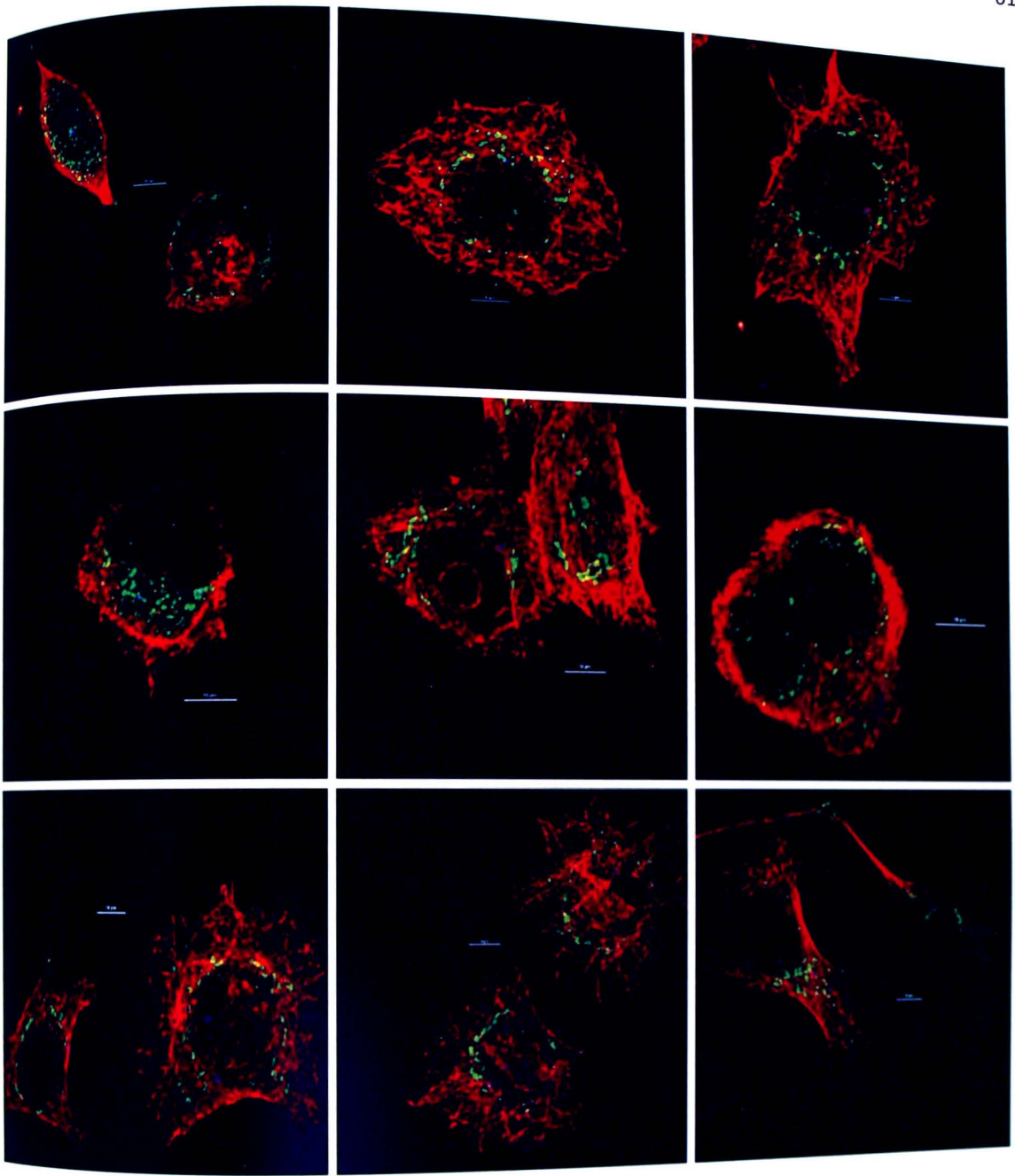


Figure 26. Control MCF-7 cells used to compare to EGF-treated cells. In addition to the image seen in figure 15, these nine images were also analyzed for colocalization between  $\alpha$ -tubulin (red) and GM130 (green), and between GM130 and  $\gamma$ -tubulin (blue). Though these cells typically form dense sheets of numerous cells, fields of view containing only 1-3 cells each were used.

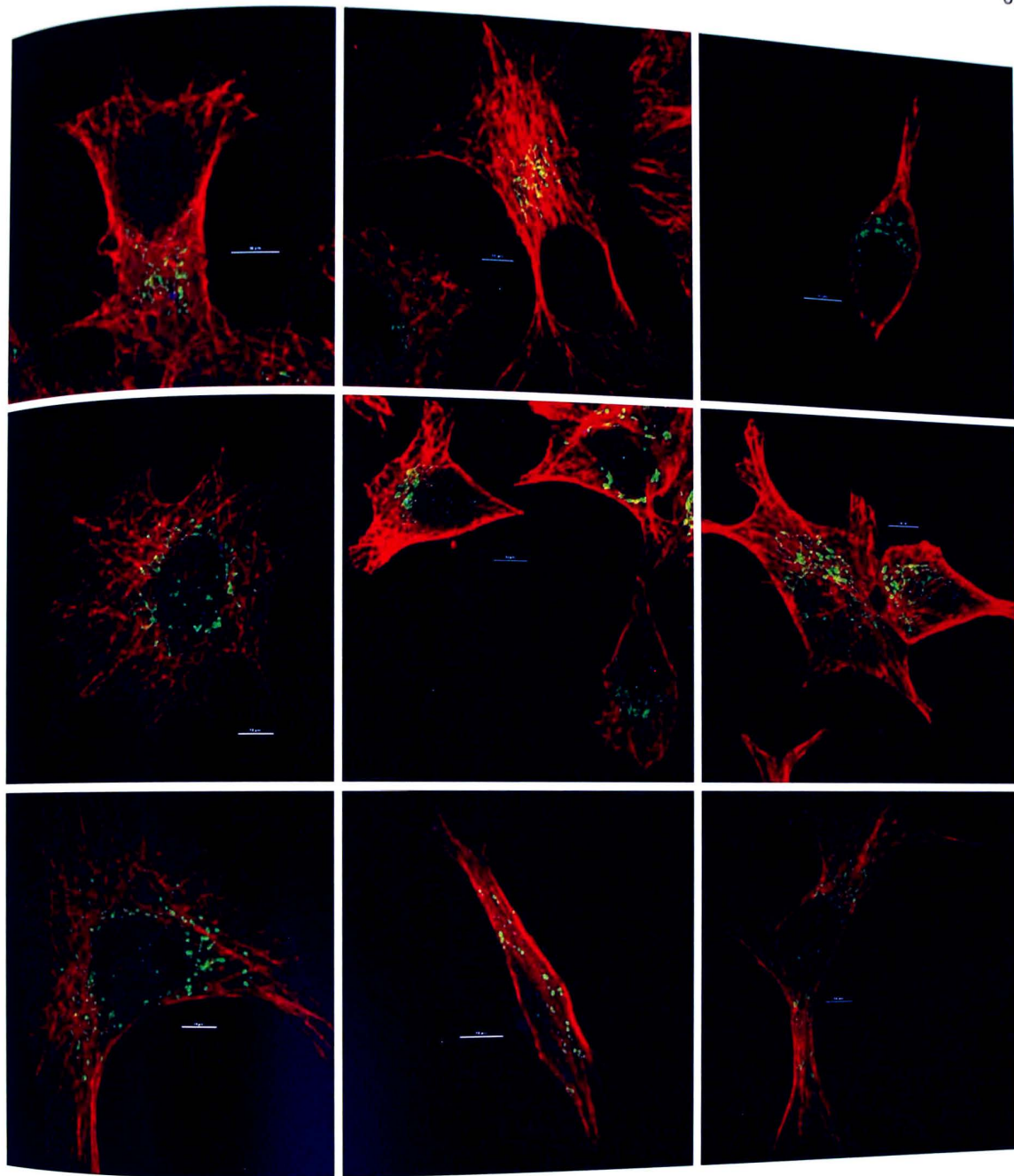


Figure 27. Additional images of EGF-treated MCF-7 cells. In addition to the image seen in figure 16, these nine images were also analyzed for colocalization between  $\alpha$ -tubulin (red) and GM130 (green), and between GM130 and  $\gamma$ -tubulin (blue). Though these cells typically form dense sheets of numerous cells, fields of view containing only 1-3 cells each were used. Scale bar represents 10 $\mu$ m.

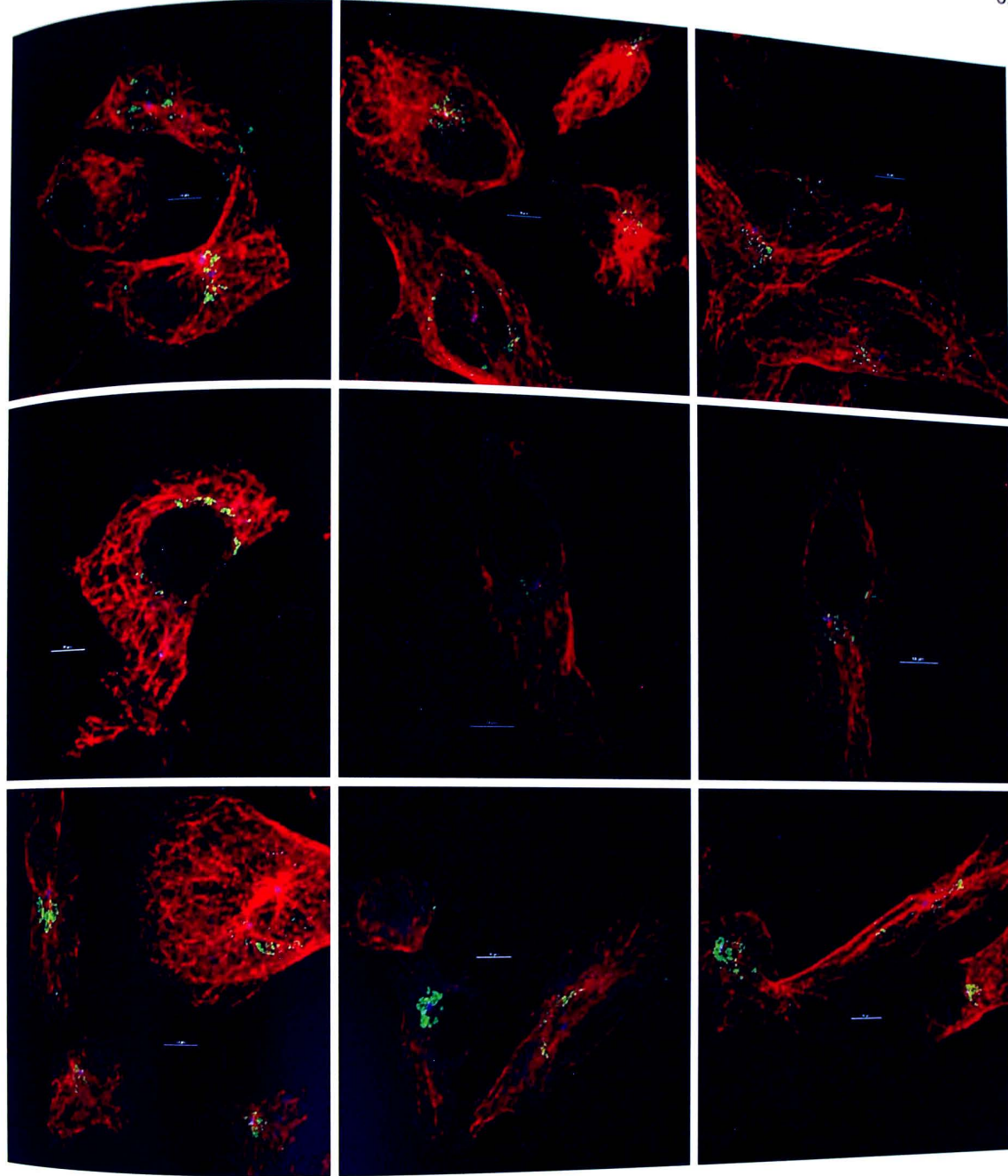


Figure 28. Control MDA-MB-231 cells used to compare to EGF-treated cells. In addition to the image seen in figure 17, these nine images were also analyzed for colocalization between  $\alpha$ -tubulin (red) and GM130 (green), and between GM130 and  $\gamma$ -tubulin (blue). Scale bar represents  $10\mu\text{m}$

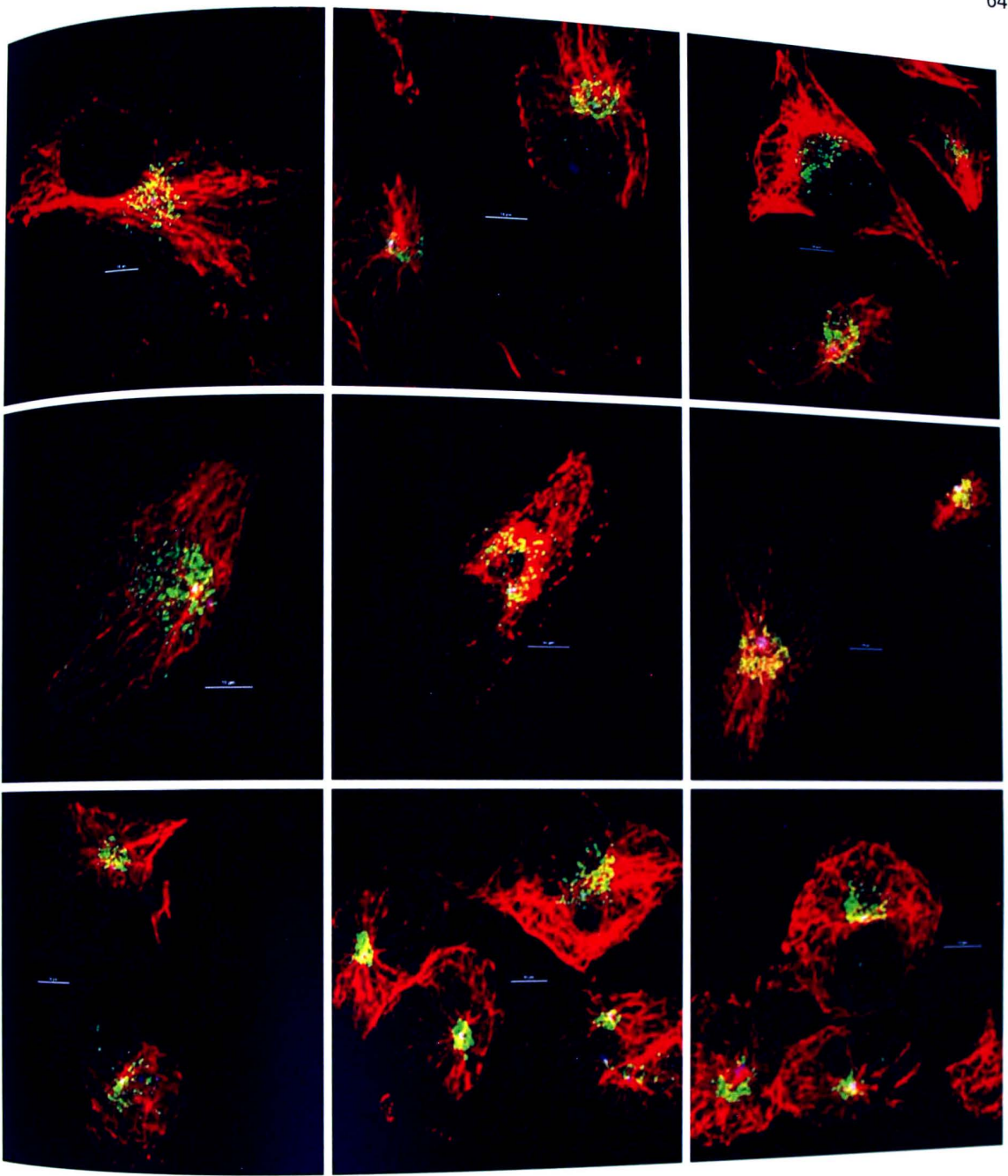


Figure 29. Additional images of EGF-treated MDA-MB-231 cells. In addition to the image seen in figure 17, these nine images were also analyzed for colocalization between  $\alpha$ -tubulin (red) and GM130 (green), and between GM130 and  $\gamma$ -tubulin (blue). Scale bar represents 10  $\mu$ m

## APPENDIX B: Data Tables

<i>Noco+Ice Regrowth</i>	red/green	green/red	green/blue	blue/green
MCF7 4m 1	0.209	0.046	0.02	0.222
MCF7 4m 2	0.246	0.122	0.013	0.284
MCF7 4m 3	0.088	0.034	0.018	0.08
MCF7 4m 4	0.148	0.152	0.023	0.115
MCF7 4m 5	0.047	0.023	0.014	0.075
<b>AVERAGE</b>	<b>0.1476</b>	<b>0.0754</b>	<b>0.0176</b>	<b>0.1552</b>
<b>St Dev</b>	<b>0.082348649</b>	<b>0.057799654</b>	<b>0.004159327</b>	<b>0.093213196</b>

<i>ICE regrowth</i>	red/green	green/red	green/blue	blue/green
MDA 40s 1	0.083	0.586	0.156	0.125
MDA 40s 2	0.065	0.792	0.125	0.1
MDA 40s 3	0.201	0.937	0.492	0.263
MDA 40s 4	0.07	0.831	0.189	0.108
MDA 40s 5	0.222	0.974	0.214	0.3
<b>AVERAGE</b>	<b>0.1282</b>	<b>0.824</b>	<b>0.2352</b>	<b>0.1792</b>
<b>St Dev</b>	<b>0.076685722</b>	<b>0.152468029</b>	<b>0.147433714</b>	<b>0.094729615</b>

<i>Noco regrowth</i>	red/green	green/red	green/blue	blue/green
MDA 60s 1	0.472	0.32	0.122	0.636
MDA 60s 2	0.473	0.162	0.343	0.25
MDA 60s 3	0.308	0.305	0.059	0.323
MDA 60s 4	0.405	0.261	0.129	0.47
MDA 60s 5	0.296	0.139	0.108	0.235
<b>AVERAGE</b>	<b>0.3908</b>	<b>0.2374</b>	<b>0.1522</b>	<b>0.3828</b>
<b>St Dev</b>	<b>0.085724559</b>	<b>0.082639579</b>	<b>0.110107675</b>	<b>0.169389197</b>

Table 5. Raw colocalization data for the MT disassembly regrowth experiments.

<i>Control</i>	red/green	green/red	green/blue	blue/green
MCF7-1	0.028	0.354	0.097	0.031
MCF7-2	0.031	0.398	0.1	0.049
MCF7-3	0.015	0.346	0.3	0.035
MCF7-4	0.015	0.513	0.205	0.01
MCF7-5	0.034	0.276	0.181	0.053
MCF7-6	0.024	0.133	0.169	0.033
MCF7-7	0.016	0.292	0.076	0.014
MCF7-8	0.012	0.704	0.321	0.016
MCF7-9	0.011	0.526	0.149	0.015
MCF7-10	0.041	0.396	0.11	0.041
<b>AVERAGE</b>	<b>0.0227</b>	<b>0.3938</b>	<b>0.1708</b>	<b>0.0297</b>
<b>St Dev</b>	<b>0.0104142</b>	<b>0.15778241</b>	<b>0.084424588</b>	<b>0.015355419</b>

<i>EGF</i>	red/green	green/red	green/blue	blue/green
MCF7 -1	0.043	0.577	0.078	0.14
MCF7 -2	0.042	0.838	0.033	0.073
MCF7 -3	0.066	0.692	0.031	0.115
MCF7 -4	0.055	0.393	0.079	0.137
MCF7 -5	0.152	0.622	0.129	0.19
MCF7 -6	0.079	0.54	0.185	0.132
MCF7 -7	0.065	0.804	0.056	0.135
MCF7 -8	0.04	0.485	0.014	0.032
MCF7 -9	0.033	0.744	0.268	0.048
MCF7 -10	0.039	0.339	0.071	0.026
<b>AVERAGE</b>	<b>0.0614</b>	<b>0.6034</b>	<b>0.0944</b>	<b>0.1028</b>
<b>St Dev</b>	<b>0.035078325</b>	<b>0.168705002</b>	<b>0.079109207</b>	<b>0.054769821</b>

Table 6. Raw colocalization data for control and EGF-treated MCF-7 cells.

Control	red/green	green/red	green/blue	blue/green
MDA-1	0.025	0.427	0.111	0.038
MDA-2	0.022	0.677	0.101	0.043
MDA-3	0.01	0.542	0.26	0.012
MDA-4	0.025	0.487	0.366	0.058
MDA-5	0.013	0.632	0.054	0.057
MDA-6	0.013	0.435	0.126	0.113
MDA-7	0.019	0.59	0.316	0.026
MDA-8	0.005	0.296	0.207	0.03
MDA-9	0.02	0.271	0.125	0.059
MDA-10	0.054	0.641	0.211	0.121
Average	<b>0.0206</b>	<b>0.4998</b>	<b>0.1877</b>	<b>0.0557</b>
St Dev	0.013459404	0.14231327	0.1018758	0.035733738

EGF	red/green	green/red	green/blue	blue/green
MDA - 1	0.071	0.995	0.011	0.373
MDA - 2	0.079	0.944	0.016	0.53
MDA - 3	0.098	0.772	0.028	0.118
MDA - 4	0.17	0.943	0.201	0.286
MDA - 5	0.277	0.956	0.034	0.982
MDA - 6	0.184	0.918	0.176	0.506
MDA - 7	0.331	0.981	0.574	0.434
MDA - 8	0.34	0.869	0.143	0.542
MDA - 9	0.303	0.703	0.297	0.555
MDA - 10	0.096	0.843	0.051	0.351
AVERAGE	<b>0.1949</b>	<b>0.8924</b>	<b>0.1531</b>	<b>0.4677</b>
St Dev	0.108881638	0.09525195	0.17639378	0.226574025

Table 7. Raw colocalization data for control and EGF-treated MDA-MB-231 cells.